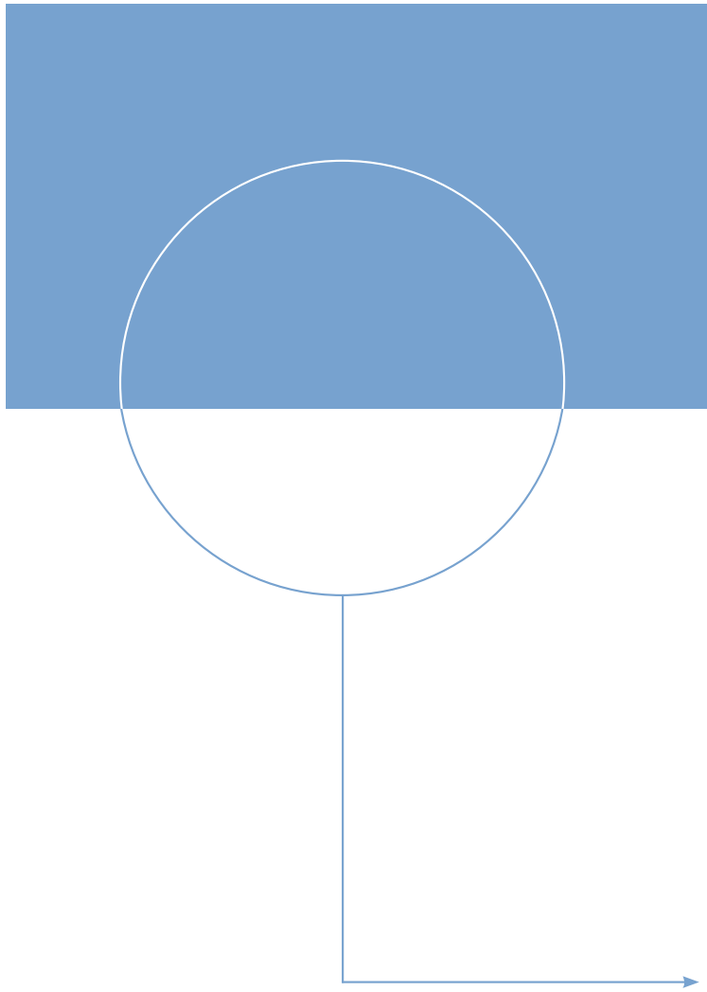

Master's thesis

2021

Anna Holm Gjeraker

NTNU
Norwegian University of
Science and Technology
Faculty of Engineering
Department of Marine Technology

Anna Holm Gjeraker

Response Amplitude Operator Estimation and Wave Modeling Sensitivity

June 2021

NTNU
Norwegian University of
Science and Technology

NTNU
Norwegian University of
Science and Technology

NTNU

Norwegian University of
Science and Technology

Response Amplitude Operator Estimation and Wave Modeling Sensitivity

Anna Holm Gjeraker

Marine Technology
Submission date: June 2021
Supervisor: Ulrik Dam Nielsen
Co-supervisor: Astrid H. Brodtkorb, Raphaël E.G. Mounet, and Petter Moen

Norwegian University of Science and Technology
Department of Marine Technology

NTNU Trondheim
Norwegian University of Science and Technology
Department of Marine Technology

MASTER OF TECHNOLOGY THESIS DEFINITION (30 SP)

Name of the candidate:	Anna Holm Gjeraker
Field of study:	Marine cybernetics
Thesis title (Norwegian):	Respons Amplitude Operator estimering of bølgemodelering sensitivitet
Thesis title (English):	Response Amplitude Operator estimation and wave modeling sensitivity

Background

The calculation of vessel responses often assumes a linear relationship between the waves and the vessel, governed by the Response Amplitude Operator (RAO). RAOs are essential in seakeeping analyses to ensure safe and energy efficient marine operations. The waves are often modeled in terms of an idealized wave spectrum, and the RAOs are usually obtained through model tests or numerical software. In more severe sea states, the assumption of small amplitude waves may not be appropriate due to nonlinear effects. Furthermore, the RAOs may not fully represent the true vessel condition due to ongoing operations that influence the vessel characteristics, or because of uncertainties in the loading condition.

This thesis aims to improve vessel response predictions by studying the sensitivity to wave modeling and estimating RAOs using two different methods. The sensitivity analysis will be applied to a full-scale construction vessel. A method for estimating a tuning coefficient, and a brute-force method, will be used to estimate the RAOs of the vessel model Cybership Inocean Cat I Drillship, abbreviated CSAD. Average RAOs will be calculated based on the sample-specific estimates, and their prediction capability evaluated on two test cases.

Scope of Work

1. Perform a background and literature review to provide information and relevant references on:
   - Background theory
     - Calculation of the wave-induced vessel response in the frequency domain
     - RAOs
     - Modeling of waves
     - Relevant optimization methods
   - Literature research
     - Uncertainties in description of the sea state.
     - Methods for estimating vessel models.
     - Methods for predicting wave-induced vessel response.

   Write a list with abbreviations and definitions of terms and symbols, relevant to the literature study and project report.
2. Extract relevant data from the full-scale dataset from Subsea 7.
3. Gather data through model tests in the Marine Cybernetics lab.
   - Preparation: familiarize equipment and software and set up a plan of test cases before every week.
   - Run CSAD in Dynamic Positioning (DP) and perform 15 minutes of measurements for every test case.
   - Calculate the RAOs of CSAD in ShipX.
   - Froude scale the experimental data to full scale.
4. Perform a sensitivity study on vessel response prediction based on the full-scale dataset.
   - Model the waves as JONSWAP-, PM-, and Ochi Hubble spectra based on wave parameters from weather forecasts.
   - Calculate the theoretical vessel response by using the numerically calculated RAOs. Compare with response measurements.

5. Implement the tuning- and observer algorithm in MATLAB and test their performances on the experimental data.
    - Estimate sample-specific RAOs for every test case of the experimental dataset by using both algorithms.
    - Calculate the average RAOs from the sample-specific RAOs.
    - Evaluate the prediction capability of the average RAOs.
    - Validate the results based on the ShipX RAOs and measured vessel responses.

Specifications

The student shall at startup provide a maximum 2-page week plan of work for the entire project period, with main activities and milestones. This should be updated on a monthly basis in agreement with supervisor.

Every weekend throughout the project period, the candidate shall send a status email to the supervisor and co-advisors, providing two brief bulleted lists: 1) work done recent week, and 2) work planned to be done next week.

The scope of work may prove to be larger than initially anticipated. By the approval from the supervisor, described topics may be deleted or reduced in extent without consequences with regard to grading.

The candidate shall present personal contribution to the resolution of problems within the scope of work. Theories and conclusions should be based on mathematical derivations and logic reasoning identifying the steps in the deduction.

The report shall be organized in a logical structure to give a clear exposition of background, problem/research statement, design/method, analysis, and results. The text should be brief and to the point, with a clear language. Rigorous mathematical deductions and illustrating figures are preferred over lengthy textual descriptions. The report shall have font size 11 pts., and it is not expected to be longer than 70 A4-pages, 100 B5-pages, from introduction to conclusion, unless otherwise agreed. It shall be written in English (preferably US) and contain the elements: Title page, abstract, preface (incl. description of help, resources, and internal and external factors that have affected the project process), acknowledgement, project definition, list of symbols and acronyms, table of contents, introduction (project background/motivation, objectives, scope and delimitations, and contributions), technical background and literature review, problem formulation, method, results and analysis, conclusions with recommendations for further work, references, and optional appendices. Figures, tables, and equations shall be numerated. The original contribution of the candidate and material taken from other sources shall be clearly identified. Work from other sources shall be properly acknowledged using quotations. The work is expected to be conducted in an honest and ethical manner, without any sort of plagiarism and misconduct, which is taken very seriously by the university and will result in consequences. NTNU can use the results freely in research and teaching by proper referencing, unless otherwise agreed.

The thesis shall be submitted with an electronic copy to the main supervisor and department according to NTNU administrative procedures. The final revised version of this thesis definition shall be included after the title page. Computer code, pictures, videos, dataseries, etc., shall be included electronically with the report.

Start date: 15 January, 2021 **Due date:** 10 June, 2021

Supervisor: Ulrik Dam Nielsen
Co-advisor(s): Astrid H. Brodtkorb, Raphaël E.G. Mounet, Petter Moen

Signatures:

Preface

This thesis is entirely written by Anna Holm Gjeraker in spring 2021 as part of the master degree in Marine Cybernetics at the Norwegian University of Science and Technology (NTNU). The work was carried out in collaboration with the company Subsea 7.

The overreaching goal of this thesis was to improve vessel response predictions based on available sea state information and vessel response predictions. A sensitivity study on response prediction was carried out, in addition to a study of two different methods for estimating the Response Amplitude Operator (RAO). The sensitivity study was applied to full-scale data of a construction vessel and weather forecasts provided by Subsea 7, which contributed as co-supervisor during both the pre-project submitted at NTNU in December 2020 [1] and the spring semester. Subsea 7 assured thorough learning of extracting the data through a digital service and support during the semester. It was highly motivating to work closely with the company and get the experience of working with actual data.

The methods for estimating the Response Amplitude Operator (RAO) were applied to the experimental data of Cybership Inocean CAT I Drillship (CSAD) gathered at the Marine Cybernetics Laboratory (MC Lab) in collaboration with Sindre Sagsveen Slåttum. The first weeks of the semester were used to prepare the model tests and familiarize the equipment and software at the laboratory. Then, model tests were conducted over four weeks. The work showed to be both intriguing and challenging, where experience from own mistakes dominated the learning process. The challenges encountered provided valuable experience on the practical aspects of the research objectives in this thesis.

Parts of the work in this thesis are based on work from the pre-project [1]. It includes the implementation of the observer algorithm for estimating the sample-specific RAOs in Python 3 language. For the purpose of this work, the algorithm was rewritten to MATLAB. The presented tuning algorithm is proposed by Nielsen et al. [2], and the research objectives were inspired by his suggestions for future work. The original code was shared by Nielsen for more efficient implementation and was adapted to generate the results in this thesis.

Due to the circumstances around COVID-19, the semester has been different than first anticipated. Since my supervisor, Ulrik Dam Nielsen, was situated at the Technical University of Denmark (DTU) during the entire period, and my co-supervisor Astrid H. Brodtkorb had maternity leave in February, challenges were especially imposed in the set-up of the model tests. However, their understanding of the situation and availability has been helpful to obtain a rewarding learning outcome from writing this thesis.

Trondheim, June 5th, 2021

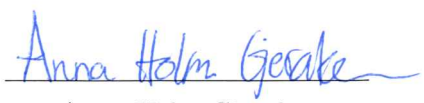

Anna Holm Gjeraker

Acknowledgements

Thank you to my supervisor Ulrik Dam Nielsen for all contributions and help to the master thesis. Ulrik has been available for questions and support on all encountered issues, and I would not have been able to solve all issues without his guidance. I would also like to thank my co-supervisors Astrid H. Brodtkorb and Raphaël E.G. Mounet for all their help. Astrid has been available for help during the spring semester, despite her maternity leave from February 2021. She was also my supervisor in the pre-project submitted in December 2020. Raphaël has given support throughout the semester, where he has answered questions and discussed issues I have encountered. He also gave his support during the model tests at the Marine Cybernetics Laboratory (MC Lab). The model tests were conducted in close collaboration with Sindre Sagsveen Slåttum. Additionally, I thank Torgeir Wahl for continuously being available for help at the MC Lab, which has been crucial for conducting the model tests. Further, thanks to Lars Øien and Marco Nataletti for all their help related to calculating the RAOs of Cybership Inocean Cat I Drillship (CSAD) in ShipX.

This thesis has been written in collaboration with Subsea 7. Therefore, thank you to Subsea 7 for sharing data and permission to publish the results. Especially thanks to Petter Moen for support in both the pre-project and the master thesis. Further, thank you to Nikolai Schjøtt-Pedersen for all the help with extracting the data and answering all my questions during the semester.

Abstract

Information about the sea state and the Response Amplitude Operator (RAO) are essential in studying the motions of floating structures. Response predictions in marine operations often rely on wave spectrum models based on statistical wave parameters provided by forecasts to describe the ocean environment. However, the choice of wave spectrum depends, among other things, on the geographical location of the vessel, the on-site wave system, and the wave parameters. Further, the RAOs are typically calculated based on linear theory by numerical methods. As a result of the increased availability of response measurements in the maritime industry, more detailed estimates of the RAOs can be obtained by utilizing measurements to capture nonlinear effects in the wave-induced response for more severe sea states. A focus on an improved representation of the sea state and vessel characteristics can provide significant benefits in terms of the safety onboard vessels and costs of an operation due to increased accuracy in response predictions.

In this thesis, the aim was to improve the prediction accuracy of vessel responses through a sensitivity study and RAO estimation. A sensitivity study of response predictions to wave modeling was conducted on full-scale data of a construction vessel. The theoretical response was calculated by utilizing the numerically calculated RAOs, and JONSWAP-, PM-, and Ochi-Hubble spectra modeled based on wave parameters from weather forecasts. The study showed that the response was sensitive to uncertainty elements of the relation between the forecasted parameters for the total wave and the wind-wave and swell components. Further, none of the considered wave spectrum models enabled to satisfactorily reproduce the measurements for all samples despite minor variations in the sea states. Additionally, two methods for estimating the RAOs of a vessel have been proposed, based on response measurements and a known wave spectrum. The tuning algorithm optimizes a tuning coefficient to improve an initial estimate of the RAOs. In contrast, the observer algorithm is based on a brute-force method for sea state estimation that requires no prior estimate of the RAOs. The methods were evaluated on data gathered at the Marine Cybernetics Laboratory (MC Lab) in Trondheim for Cybership Inocean Cat I Drillship (CSAD). The sample-specific estimates from the dataset were utilized to calculate average RAOs with respect to the significant wave height. Due to a limited dataset with wave energies distributed for frequencies where the wave-induced response is expected to be low, the results showed that the estimated RAOs do not reflect the true physics of the vessel. Further, the average RAOs showed a clear dependence on the individually estimated responses due to few samples. However, good agreement was seen when the average RAOs were used to predict the vessel response for two sea states, despite the unrealistic RAO estimates.

Sammendrag

Informasjon om sjøtilstanden og Respons Amplitude Operator (RAO) er viktig for å studere bevegelsene til flytende strukturer. Responsprediksjoner i marine operasjoner er ofte avhengige av bølgespektrummodeller basert på statistiske bølgeparametere gitt av værprognoser for å beskrive havmiljøet. Valget av bølgespektrum avhenger imidlertid blant annet av fartøyets geografiske beliggenhet, bølgesystemet, og bølgeparameterne. Videre blir RAOer vanligvis beregnet basert på lineær teori ved hjelp av numeriske metoder. Som et resultat av den økte tilgjengeligheten av responsmålinger i den maritime industrien, kan mer detaljerte RAO estimat oppnås ved å bruke målinger for å fange opp ulineære effekter i den bølgeinduserte responsen for høyere sjøtilstander. Fokus på en forbedret representasjon av sjøtilstanden og fartøysegenskapene kan gi betydelige fordeler når det gjelder sikkerheten ombord på fartøy og kostnader ved en operasjon på grunn av økt nøyaktighet i responsprediksjoner.

Målet i denne oppgaven var å forbedre prediksjonsnøyaktigheten av fartøyresponser gjennom en sensitivitetsstudie og RAO-estimering. En sensitivitetsstudie av responsprediksjon til bølgemodellering ble utført på fullskala data fra et konstruksjonsfartøy. Den teoretiske responsen ble beregnet ved å bruke de numerisk beregnede RAOene, og JONSWAP-, PM- og Ochi-Hubble-spektrene modellert basert på bølgeparametere fra værprognoser. Studien viste at responsen var sensitiv for de usikre elementene i forholdet mellom de prognostiserte parameterne for totalbølgen og vind- og dønning komponentene. Videre var ingen av de vurderte bølgespektrummodellene i stand til å tilfredsstillende gjengi alle målingene til tross for små variasjoner i sjøtilstandene. I tillegg er det foreslått to metoder for å estimere RAOene til et fartøy, basert på responsmålinger og et kjent bølgespektrum. Tuning-algoritmen optimaliserer en tuning-koeffisient for å forbedre et initielt estimat av RAOene. I motsetning er observer-algoritmen basert på en brute-force-metode for estimering av sjøtilstander som ikke krever noe tidligere estimat av RAOene. Metodene ble evaluert på data samlet ved Laboratoriet for Marin Kybernetikk (MC Lab) i Trondheim for Cybership Inocean Cat I Drillship (CSAD). De individuelle estimatene for hver modelltest ble brukt til å beregne gjennomsnittlige RAOer med hensyn til intervall av signifikante bølgehøyder. På grunn av et begrenset datasett med bølgeenergier distribuert for frekvenser der det forventes at bølgeindusert respons er lav, viste resultatene at de estimerte RAOene ikke gjenspeiler fartøyets sanne fysikk. Videre viste de gjennomsnittlige RAOene en klar avhengighet av de individuelle responsestimatene som følge av et begrenset antall tester. Imidlertid så man god overensstemmelse når de gjennomsnittlige RAOene ble brukt til å predikere fartøyets respons for to sjøtilstander, til tross for de urealistiske RAO-estimatene.

Contents

Acronyms

CAD	Computer Aided Design.
CNN	Convolutional Neural Network.
cRIO	CompactRIO.
CSAD	Cybership Inocean Cat I Drillship.
DFT	Discrete Fourier Transform.
DoF	Degree of Freedom.
DP	Dynamic Positioning.
DWS	Directional Wave Spectrum.
ECMWF	European Center of Median-Range Weather Forecasts.
EoM	Equation of Motion.
FPSO	Floating Production, Storage, and Offloading.
HTF	Hydrodynamic Transfer Function.
IMU	Inertial Measurement Unit.
JONSWAP	Joint North Sea Wave Project.
LNG	Liquefied Natural Gas.
LSTM	Long-Short-Term-Memory.
MC Lab	Marine Cybernetics Laboratory.
NED	North-East-Down.
NI	National Instruments.
NTNU	Norwegian University of Science and Technology.
OSV	Offshore Supply Vessel.
PM	Pierson-Moskovitz.
PSD	Power Spectral Density.
R^2	Square Correlation Coefficient.
RAO	Response Amplitude Operator.

RMS	Root Mean Square.
RMSE	Root Mean Square Error.
RRN	Recurrent Neural Network.
SISO	Single Input Single Output.

1 Introduction

Wave-induced responses are often predicted by seakeeping analysis based on linear theory through a description of the vessel characteristics utilizing a Response Amplitude Operator (RAO). As such, RAOs are essential in studying the motions of floating structures in ship-design projects and during marine operations to ensure the desired safety and efficiency for execution. However, the sea state is of equal importance in the numerical prediction, often given in terms of the wave spectrum.

1.1 Motivation

The accuracy of RAOs and the sea state, and thereby the response prediction accuracy, is a crucial factor for operators to reduce downtime and costs of an operation. The RAOs are traditionally calculated for different loading conditions by numerical software based on panel methods or strip theory that require detailed information about the hull lines [1]. This information may not be available in the design stage of a vessel, hence assumptions must be taken in the calculation. At later stages, the hull lines are typically restricted to a limited number of stakeholders. They may not be available for the ship operator to obtain updated RAOs for the given operation. Updated RAOs could also be beneficial in operations with changing loading conditions, like pipe-laying or lifting operations.

Waves can be directly measured by instruments like wave buoys and radars, and post-processed to obtain the wave spectrum at the desired location. Wavefield data is also frequently obtained from weather forecasts in terms of statistical wave parameters predicted by numerical models. The wave spectrum can then be modeled as one of different idealized wave spectra derived from experimental studies. However, spectrum accuracy correlates with the parameter accuracy, and the choice of the model impacts the wave energy distribution. Uncertainties related to wave forecasts are studied by Orimolade et al. [2] by comparing deterministic forecasts for a location in the Barents Sea and the Norwegian Sea against measurements at the corresponding location. The comparison study showed that the uncertainty varies with location and season.

In recent years, installing sensors on vessels and offshore structures has increased the data available in the maritime sector, motivating decision-making through vessel modeling and simulations. It is seen in embedded systems like decision support systems, where data plays an essential role in ensuring safe navigation and support for the crew. Digital twins have also gained interest in the maritime industry, where low-cost analyses are carried out to predict vessel behaviors during operations. A similarity for both examples is the common use of the first principle methods utilizing models like RAOs for response prediction. Since vessel RAOs cannot themselves be measured directly, researchers have proposed methods that exploit the available data to estimate RAOs based on response measurements and knowledge of the on-site wave conditions. Some of the methods are introduced below and aim to improve the accuracy of traditionally RAOs calculated based on linear theory to

account for nonlinear effects in the wave-induced response for more severe sea states.

The method proposed by Skandali et al. [3] is an example where RAOs are calibrated using vector fitting. In contrast, Han et al. [4, 5] aim at improving the RAO accuracy by hydrodynamic model parameter tuning based on two different approaches. The first method is based on spectral analysis, probabilistic modeling, and the discrete Bayesian updating formula. The second method is shown to be much more efficient by tuning the parameters based on the unscented transformation and scaled unscented Kalman filter.

An increased interest has also been seen in response prediction based on data-driven methodologies. The methods benefit from their independence of the RAOs, hence reducing challenges related to changing vessel characteristics during operation. Gilbert et al. [6] studies a method to improve access forecasting for offshore wind farm operations using a data-driven methodology. The best performing model is trained to estimate vessel motion up to 5 days ahead based on heave peak-to-peak displacement measurements and sea state parameters. Nielsen et al. [7] study a semi-empirical model for added-wave resistance estimation, where improved estimates are valuable in terms of energy efficiency in the shipping industry and the risk of designing under-powered ships.

A challenge related to the examples based on historical motion records is their ability to obtain generalized estimates. This means that an estimated RAO from previous samples may not be valid during the entire operation if the condition changes. Therefore, a real-time procedure is required to continuously update the RAO estimates based on new input. In situations where real-time estimation procedures are not suited, accurate estimations of generalized RAOs may be obtained by calculating the average RAO over a given number of sample-specific estimates. This is beneficial when it is desired to improve existing RAOs, or if the RAOs are initially unknown.

1.2 Research Objectives

This thesis is completed in collaboration with the company Subsea 7 and has two different objectives with an overreaching goal of improving vessel response predictions based on available sea state information and vessel response measurements. Firstly, a sensitivity study on the predicted response will be assessed utilizing full-scale measurements of a vessel and wave spectral parameters provided by external weather forecasts. Since actual 2D wave spectra measurements are not available, the prediction sensitivity will be evaluated by modeling the wave spectrum using three different parametrized 1D spectra. Secondly, two methods for estimating the RAO for heave and pitch motion are studied based on experimental data obtained at the Marine Cybernetics Laboratory (MC Lab) located at the Center of Marine Technology in Trondheim. Both methods require vessel response measurements for heave and pitch as input and wave spectral parameters in terms of the significant wave height, peak period, and wave direction. The aim is to generalize the RAO estimates by calculating the average RAOs for a pre-defined range of significant wave heights. Though individually evaluated, the methods will be compared to form an

idea of the future potentials of implementation.

1.3 Main Contributions

A sensitivity study on vessel response prediction for heave and pitch motion is conducted by calculating the theoretical response based on available RAOs and wave spectra. Additionally, two methods for estimating the RAOs are implemented, tested, and evaluated to represent a diverse selection of methodologies to obtain an improved knowledge of the wave-ship interaction for a given vessel. The first method is an extension of the pre-project submitted by the author in December 2020 at the Norwegian University of Science and Technology (NTNU) [8]. It considers an iterative approach that utilizes the residual between the measured and estimated vessel responses assuming no prior knowledge of the RAOs. The second method is proposed by Nielsen et al. [1] for estimating a tuning coefficient employing least-squares optimization. The tuning coefficient updates an initial estimate of the RAOs calculated by semi-analytical closed-form expressions.

1.4 Organization of the Thesis

The remainder of the thesis is organized as follows.

Section 2: Presents the necessary background theory for understanding frequency domain calculation of vessel response, in addition to an explanation of a selection of optimization algorithms used for implementing the methods.

Section 3: Presents previous work in the field of sea state description uncertainties, vessel model estimation, and response prediction.

Section 4: Presents the methods proposed in this thesis. This entails definitions and assumptions, the datasets used for testing, the sensitivity analysis on wave spectrum modeling, and the two algorithms for estimating the RAOs.

Section 5: Evaluates and discusses the results. Results from the sensitivity study is first presented, followed by the results from the estimation algorithms.

Section 6: Discusses the implications of the sensitivity analysis in terms of vessel response prediction, and the implications and uses of the two individual methods for estimating an average RAO with respect to ranges of significant wave heights.

Section 7: Concludes on the influence of wave spectrum modeling on vessel response predictions, and the methods studied for RAO estimation.

Appendix A: Presents the derivation of the semi-analytical closed-form expressions for the RAOs used by the tuning algorithm.

2 Theory

The theory in this section aims to provide the necessary background knowledge for understanding the methods studied in this thesis. The first part focuses on the frequency-domain analysis of the wave-induced vessel response and describes the RAOs and response spectra. Then, different idealized spectra are explained, followed by theory about different optimization methods. The first part is based on work from the pre-project [8].

2.1 Wave-induced Vessel Response

Dynamic analyses are essential for evaluating a vessel's seakeeping capabilities in the design stages and operations. The processes involved in the analyses is the ocean environment and wave-induced responses, described in terms of their statistical properties to account for the stochastic variation in the loads. These processes can be analyzed in the time-domain, or the frequency-domain [9]. The statistical variability is commonly described in terms of short-term statistics regarding stationary Gaussian processes where the sea surface elevation is assumed to be the only time-varying parameter. In the time domain, the wave-induced vessel response is modeled as time series, or samples, over set time frames. In the frequency domain, the Gaussian process is described by the signal's power distribution as a function of frequency.

The wave-induced vessel response can be modeled in terms of a RAO and wave spectrum, assuming linear theory and stationary conditions. In a spectral formulation, the steady-state responses induced by the wave system are given by the cross-spectrum

$$S_{R,ij}(\omega,\beta) = \int X_i(\omega,\beta)\overline{X_j(\omega,\beta)}S_\zeta(\omega,\mu)d\mu, \tag{1}$$

for a pair (i,j), defined as the Degree of Freedom (DoF) in heave and pitch given as $i,j = \{z,\theta\}$, respectively [10]. $X_i(\omega,\beta)$ is the motion transfer function and $\overline{X_j(\omega,\beta)}$ its complex conjugate for the wave frequencies, ω, and the relative direction, $\beta = \mu + \psi$, between the wave direction for the single waves, μ, and the vessel heading, ψ. Furthermore, $S_\zeta(\omega,\mu)$ is the two-dimensional wave spectrum. Eq.(1) is complex-valued due to imaginary parts of the motion transfer function associated with the phase angle of the response [10]. The imaginary part is zero when $i = j$, and a real-valued cross-spectrum is obtained.

2.1.1 The Surface Elevation - Frequency to Time-domain

The sea state is expressed in the time-domain by deriving an expression for the wave elevation. The wave amplitude, ζ_a, for component k is related to the wave spectrum by Eq.(2), which sums up the spectral density, $S_\zeta(\omega_k)$, for each frequency interval, $\Delta\omega$ [11].

$$\frac{1}{2}\zeta_a^2 = S_\zeta(\omega_k)\Delta\omega \tag{2}$$

Assuming that the waves propagate in one direction, the wave elevation is modeled as a long-crested irregular sea. This is obtained by summing all N harmonic components

$$\begin{aligned}\zeta &= \sum_{k=1}^{N} \zeta_a \cos(\omega_k t + \epsilon_k) \\ &= \sum_{k=1}^{N} \sqrt{2S_\zeta(\omega_k)\Delta\omega}\cos(\omega_k t + \epsilon_k).\end{aligned} \tag{3}$$

Eq.(2) is substituted in the last equality. ϵ_k is the random phase angle of the corresponding wave component.

In reality, waves propagate in multiple directions and are termed as short-crested irregular sea. The effect of multiple directions is accounted for by introducing a spreading function $f(\beta)$ to represent the 2D wave spectrum as

$$S_\zeta(\omega, \beta) = S_\zeta(\omega) f(\beta), \tag{4}$$

where β is the relative direction between vessel heading and wave direction [11]. By considering a frequency- and direction interval of $\Delta\omega$ and $\Delta\beta$, respectively, the wave elevation for a short-crested irregular sea is found as the sum of N components and M directions

$$\zeta = \sum_{k=1}^{N}\sum_{i=1}^{M} \sqrt{2S_\zeta(\omega_k, \beta_i)\Delta\omega\Delta\beta}\cos(\omega_k t + \epsilon_k). \tag{5}$$

2.1.2 Motion Response Amplitude Operators

The RAO is frequently used to obtain a measure of vessel response in a sea state and describes the ratio of ship motion amplitude to wave amplitude. The name RAO is often used in seakeeping and is closely related to transfer functions but do not encompass the phase lag [12].

By assuming linear theory and steady-state response, the motion response in irregular sea is obtained through superpositioning of regular waves with different amplitudes, wavelengths, and propagation directions [13]. The body motions are then evaluated by solving the Equation of Motion (EoM) for a rigid ship in six DoFs, $j, k = \{x, y, z, \phi, \theta, \psi\}$

$$\sum_{k=1}^{6} \left[\left(M_{jk} + A_{jk}(\omega)\right) \ddot{\eta_k} + B_{jk}(\omega)\dot{\eta_k} + C_{jk}\eta_k \right] = F_j e^{-i\omega t}. \tag{6}$$

The left side of Eq.(6) includes the vessel mass, M_{jk}, and hydrodynamic loads identified as added mass-, damping-, and restoring forces, A_{jk}, B_{jk}, and C_{jk} respectively. On the

right hand side, F_j is the complex amplitudes of the excitation loads, and the real part of $F_j e^{-i\omega t}$ denotes the force and moment components [13]. For a wave with frequency ω and direction β, the excitation load can be expressed as the linear relation

$$F_j e^{-i\omega t} = \zeta_a X_j(\omega, \beta) e^{-i\omega t}, \tag{7}$$

between the wave amplitude, ζ_a, and the complex-valued transfer function for the excitation loads, $X_j(\omega, \beta)$. Introducing the complex notation of body motions

$$\eta_k = \eta_{ka} e^{-i\omega t}, \tag{8}$$

the solution of the EoMs is solved by substituting Eq.(8) into Eq.(6), giving the body motion system

$$\sum_{k=1}^{6} \left[-\omega^2 \left(M_{jk} + A_{jk}(\omega) \right) + i\omega B_{jk}(\omega) + C_{jk} \right] \eta_{ka} = \zeta_a X_j(\omega, \beta). \tag{9}$$

Dividing on ζ_a, the transfer function describing the amplitude and phase of the body motions relative to the waves becomes

$$\mathbf{H}(\omega, \beta) = \frac{\eta_a}{\zeta_a} = \left[-\omega^2 \left(\mathbf{M} + \mathbf{A}(\omega) \right) + i\omega \mathbf{B}(\omega) + \mathbf{C} \right]^{-1} \mathbf{X_j}(\omega, \beta), \tag{10}$$

where the RAO is given as the real part, $|H(\omega, \beta)|$.

2.1.3 Response Spectrum

The response spectrum results from the transformation of wave energy to response energy of a vessel in the frequency-domain by using Eq.(1). Figure 1 shows a principle sketch of the transformation in heave, where the transfer function is represented by the motion RAO. The wave spectrum, $S_\zeta(\omega)$, is shown to the left in Figure 1. Regular wave components associated with their corresponding wave energy, $\frac{1}{2}\zeta_a^2$, are superpositioned to describe the irregular wave history, $\zeta(t)$.

Figure 1 also shows the the response spectra for heave motion, denoted as $S_z(\omega)$. The response components are obtained by multiplication of each wave component with the motion RAO, and superpositioned to obtain the irregular response history in heave, $z(t)$.

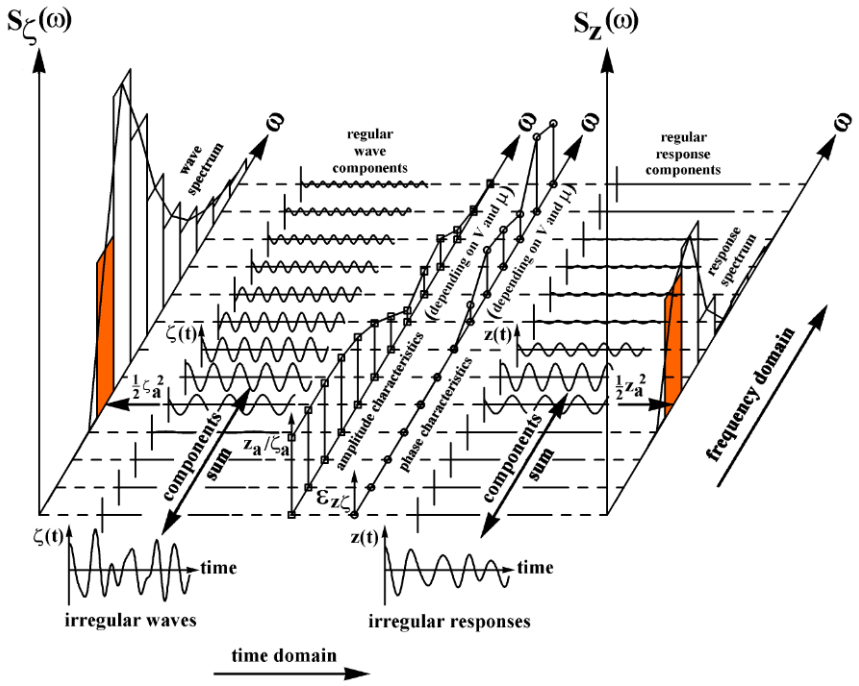

Figure 1: Transformation of wave energy to vessel response in heave [14]. $S_\zeta(\omega)$ is the wave spectrum, and $S_z(\omega)$ is the heave response spectrum.

2.2 Modeling of Waves

In situations where measurements of the actual wave conditions for a given geographic location are not available, the waves can be described in terms of their statistical properties as a sum of regular wave components [9]. Standardized wave spectra derived from experimental data are used to approximate the sea state utilizing statistical parameters like the significant wave height, H_s, and peak wave period, T_p, obtained by, among other things, weather forecasts or hindcasts. If wind-waves or swells dominate the sea state, a one-peaked spectrum like the Joint North Sea Wave Project (JONSWAP) or Pierson-Moskovitz (PM) spectrum is typically chosen. When low-frequency swells significantly influence the high-frequency wind-waves, a bimodal spectrum like the Ochi-Hubble spectrum can be used to account for the individual contributions to the total wave energy [15].

The chosen wave spectrum can be described by the spectral moments

$$m_n = \int_0^\infty \omega^n S_\zeta(\omega) d\omega, \tag{11}$$

where $S_\zeta(\omega)$ is the 1D wave spectrum for wave frequencies ω [9]. The 0-th order spectral moment is found for $k = 0$ as the standard deviation of the wave spectrum, and is essential for expressing the statistical parameters of the considered spectrum. The mentioned parametrized wave spectra and some important relations in terms of wave modeling are

described in the following sections.

2.2.1 Pierson-Moskowitz Spectrum

For fully developed sea states and unlimited fetch, the PM spectrum is described by the spectral density

$$S_\zeta(\omega) = \frac{A}{\omega^5}\exp[-\frac{B}{\omega^4}], \tag{12a}$$

$$A = 0.0081g^2, \tag{12b}$$

$$B = 0.74\left(\frac{g}{V_{wind}}\right)^4, \tag{12c}$$

where ω is the angular wave frequency, g is the gravitational constant, and V_{wind} is the wind speed at 19.5 m altitude [9]. The spectral parameters, A and B, define the type of PM spectrum. Different spectral formulations can be obtained by changing these parameters.

2.2.2 JONSWAP Spectrum

As a result of the Joint North Sea Wave Project (JONSWAP), the spectral density of the JONSWAP spectrum is described by

$$S_\zeta(\omega) = \alpha\frac{g^2}{\omega^5}\exp[-\frac{5}{4}\left(\frac{\omega_p}{\omega}\right)^4]\gamma^{\exp[-\frac{1}{2}\left(\frac{\omega-\omega_p}{\sigma\omega_p}\right)^2]} \tag{13}$$

[9]. Here, g is the gravitational constant, α determines the spectrum shape in the high frequency range, and γ is given as the ratio of the maximum spectrum energy to the maximum energy in the PM spectrum. Furthermore, σ describes the width of the left and right side of the peak, as shown in Figure 2 [16]. Since the JONSWAP spectrum describes not fully developed seas, the spectral density function is more peaked than the PM spectrum.

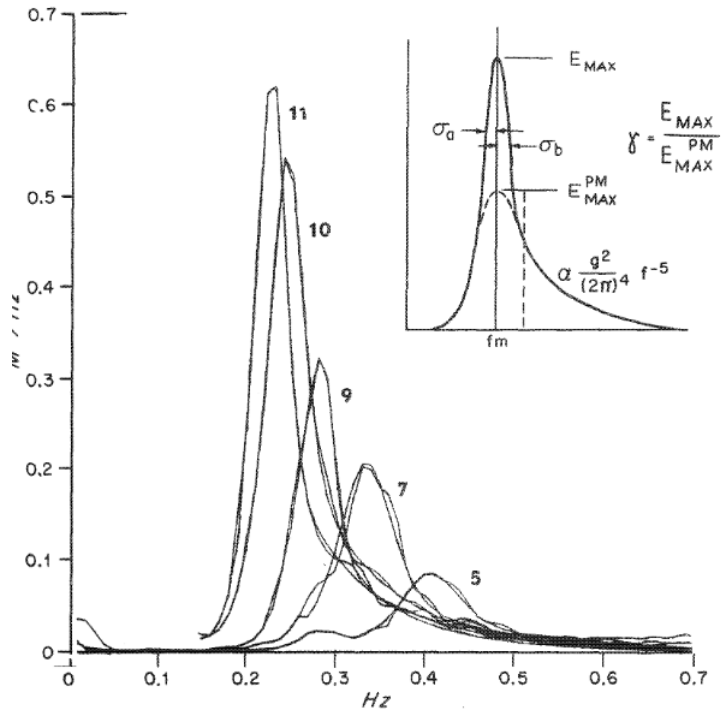

Figure 2: Measured wave spectra under ideal conditions and parametrical approximations. Principal sketch of the peak shape parameters γ, σ_a, σ_b [16].

2.2.3 Ochi-Hubble Spectrum

Ochi and Hubble describe a bimodal spectrum as the sum of two PM spectra by

$$S_\zeta^+(\omega) = \frac{1}{4}\sum_{i=1}^{2} \frac{((\lambda_i + 1/4)\omega_{p,i}^4)^{\lambda_i}}{\Gamma(\lambda_i)} \frac{H_{m0,i}^2}{\omega^{4\lambda_i+1}} \exp\left(\frac{-(\lambda_i + 1/4)\omega_{p,i}^4}{\omega^4}\right) \tag{14}$$

[15]. For the low and high frequency component, $i = 1, 2$, the significant wave height, peak frequency, and spectral shape parameter are described by $H_{m0,i}$, $\omega_{p,i}$, and λ_i, respectively. The parameters in Eq.(14) are determined in terms of empirical constants obtained from an analysis of 800 spectra based on data from the North Atlantic. Given H_{m0}, the parameters can be found by

$$H_{m0,1} = R_{p,1} H_{m0}, \tag{15a}$$

$$H_{m0,2} = \sqrt{1 - R_{p,1}^2} H_{m0}, \tag{15b}$$

$$\omega_{p,i} = a_i \exp\left(-b_i H_{m0}\right), \tag{15c}$$

$$\lambda_i = c_i \exp\left(-d_i H_{m0}\right), \tag{15d}$$

where a_i, b_i, c_i, d_i, and $R_{p,1}$ are empirical constants.

2.3 Optimization

Optimization is a tool that, among other things, can be used for analyzing physical systems based on a construction of an appropriate model. The process of modeling the system is based on identifying an objective to be maximized or minimized. The objective is determined as a scalar function f of the unknown variables x. The goal is to find the variables that yield the optimum value of the objective, given a set of constraints, c_i, on the variables that must be satisfied [17]. Mathematically, an optimization problem is defined as

$$\begin{aligned} \min_{x \in \mathbb{R}^n} \quad & f(x) \\ \text{subject to} \quad & c_i(x) = 0,\ i \in \mathcal{E}, \\ & c_i(x) \neq 0,\ i \in \mathcal{I}, \end{aligned} \tag{16}$$

where $\mathcal{E}$ and $\mathcal{I}$ are the sets of equality and inequality constraints, respectively. $x \in \mathbb{R}^n$ is a vector with $n \neq 1$ unknown variables. In unconstrained optimization, $\mathcal{E} = \mathcal{I} = \emptyset$, meaning that the constraints are disregarded. This applies to systems where the solution is not affected by any constraints.

In unconstrained optimization, an initial guess of the variables, x_0, is supplied to the algorithm. The optimization algorithm then decides the trajectory from one iterate to the next by using information about f at the current iterate x_k in search of a lower function value.

2.3.1 The Line Search Method

The line search method is one of the fundamental methods for iteration from the current point, x_k, to the next, x_{k+1}, given by

$$x_{k+1} = x_k + \alpha_k p_k \tag{17}$$

[17]. The iteration step is defined in terms of a search direction, p_k, and a step length, α_k, found by the algorithm. The line search strategy often define the search direction as

$$p_k = -B_k^{-1} \nabla f_k, \tag{18}$$

with a requirement of p_k to be a descent direction. This guarantees a reduction in f along the direction. In Eq.(18), B_k is a symmetric and nonsingular matrix, and ∇f_k is the function gradient. The step length can be found by solving the minimization problem

$$\min_{\alpha > 0} \quad f(x_k + \alpha p_k). \tag{19}$$

Newton's method is an example of a line search strategy that defines B_k as the exact Hessian $\nabla^2 f_k$, and uses the Newton direction

$$p_k^N = -(\nabla^2 f_k)^{-1} \nabla f_k, \tag{20}$$

derived from the second-order Taylor series approximation

$$f(x_k + p) \approx f_k + p^T \nabla f_k + \frac{1}{2} p^T \nabla^2 f_k p = m_k(p). \tag{21}$$

It is found as the direction p that minimizes Eq.(21). The Newton's direction require the Hessian to be positive definite, and typically uses a step length of $\alpha_k = 1$.

2.3.2 The BFGS Method

The Quasi-Newton methods provide alternative line search methods that do not require computations of the Hessian. Instead, an approximation of the Hessian, B_k, is updated at each iteration step [17]. This makes the Quasi-Newton methods only require the gradient of the objective function to account for changes during the step, thus providing information about the Hessian along the search direction.

The BFGS method is the most popular Quasi-Newton method, which updates B_k in Eq.(18) at every iteration [17]. It is based on the quadratic model of the objective function

$$m_k(p) = f_k + \nabla f_k^T p + \frac{1}{2} p^T B_k p, \tag{22}$$

where the minimizer p_k is given by Eq.(18). At each iteration, B_k is updated to satisfy the construction of a new quadratic model $m_{k+1}(p)$. Instead of imposing conditions on the Hessian approximation, the BFGS algorithm considers their inverses H_k. A unique solution of H_{k+1} is determined by solving the following problem.

$$\begin{aligned} \min_{H} \quad & \|H - H_k\| \\ \text{subject to} \quad & H = H^T,\ Hy_k = s_k \end{aligned} \tag{23}$$

In Eq.(23), H is the inverse Hessian at iterate $k+1$ to be determined as the symmetric matrix closest to the current matrix H_k. Further, $s_k = x_{k+1} - x_k$ and $y_k = \nabla f_{k+1} - \nabla f_k$ is the displacement and change of gradient, and must satisfy the curvature condition given as

$$s_k^Y y_k > 0. \tag{24}$$

If the curvature condition holds, the approximated inverse Hessian, H_{k+1}, maps y_k into s_k by the secant equation

$$H_{k+1}y_k = s_k. \tag{25}$$

In Eq.(23), the BFGS algorithm uses the weighted Frobenius norm, yielding the unique solution

$$H_{k+1} = (I - \rho_k s_k y_k^T)H_k(I - \rho_k y_k s_k^T) + \rho_k s_k s_k^T, \tag{26}$$

to Eq.(23) where $\rho_k = \frac{1}{y_k^T s_k}$.

2.3.3 Least-squares Problems

In the search of the unknown variables of an optimization problem like Eq.(16), the objective function must be defined. Least-squares problems are recognized by the quadratic objective function

$$f(x) = \frac{1}{2}\sum_{j=1}^{m} r_j^2(x), \tag{27}$$

where the residual, r_j, is a smooth function from $\mathbb{R}^n$ to $\mathbb{R}$ [17]. r_j measures the discrepancy between the observed data y_j and the behavior of a parametrized model, $\phi(t_j; x)$ as

$$r_j(x) = y_j - \phi(t_j; x), \quad j = 1, 2, ..., m. \tag{28}$$

The best-fitting parameters for the model are obtained by solving Eq.(16) in terms of the objective function in Eq.(27). Such models are considered the largest source of unconstrained optimization problems due to their relatively easy and inexpensive calculation of the Hessian, where the most important part is described in terms of the Jacobian matrix.

3 Previous Work

A literature review covering the topics related to the theory presented in Section 2 is presented here. It includes previous work focusing on uncertainties in sea state description, estimation of vessel models, and prediction of wave-induced vessel response. The mentioned topics are fundamentally based on the relationship between vessel response and the surrounding waves to improve knowledge of the on-site operational or sea state conditions. Parts of this section are based on work from the pre-project submitted in December 2020 [8].

3.1 Uncertainties in Sea State Description

For marine operations dominated by waves, the sea state description influences the numerical analyses of vessel response predictions. The local wave conditions are often provided by weather forecasts in terms of statistical parameters, requiring the spectral model to be chosen by the analyst. In situations where sea state measurements are not available, it may be challenging to validate the predicted responses that depend on the wave spectral model and estimate the bias and uncertainty of the given method. According to Guedes Soares [18], it is necessary to describe the sources of the fundamental, statistical, and model uncertainty for the probabilistic sea state description to be complete. This includes uncertainties in the spectral shape definitions such as degree of development, combined sea states, and the adequacy of standardized wave spectra.

Li et al. [19] study the effect of uncertainties in sea state description on the assessment of operational limits for two floating crane vessels, a heavy-lift vessel, and a semi-submersible. A JONSWAP- and a Torsethaugen spectrum is used to model the waves as both long-crested and short-crested. Considering the vertical crane tip motion as the critical parameter, the study shows that the corresponding response spectra and the operational limits are sensitive to the spectral models due to their different spectral distribution. Further, the estimated operational limits tend to be more conservative for short-crested waves compared to long-crested waves.

A methodology to assess uncertainties in operational limits due to the variability in wave spectral energy distribution is presented by Guachamin-Acero and Li [20]. Among other things, uncertainties are introduced in offshore sites where a combination of wind seas and swells are present in the sea state. Inaccurate partitioning of wave parameters to simplify the information result in analytical 2D wave spectra that cannot represent the actual wave condition in situations where the wave information is not adequately described. The methodology has been applied on a case study of an offshore wind turbine transition piece installation, and significant differences in operational limits are observed when uncertainties in wave spectral parameters are included.

Different considerations apply for ship model testing where a wavemaker generates waves in a basin with limited dimensions. In this case, the irregular wave properties are nor-

mally defined by a type of spectrum with corresponding significant wave height and peak period. In a published report by the International Towing Tank Conference (ITTC) [21], a procedure of uncertainty analysis for experimental ship model measurements and testing is summarized. Kim and Hermansky [22] consider the uncertainties in seakeeping experiments, introducing the details of the ITTC's procedure. It is seen that although wave parameters are considered a significant contribution to the experimental error, such uncertainties are difficult to estimate and are usually neglected. This considers wave generator limitations, deterioration of wave properties along the facilities, and reflections from wave energy dampers. Although such uncertainties are generally sufficient in engineering practice, the understanding helps evaluate experimental results.

Extending upon the issue of uncertainties in the sea state description, researchers have gained interest in estimating the sea state parameters or the wave spectrum based on both model- and non-model based calculation. Model based methods typically relate vessel response measurements to the sea state in terms of a mathematical model referred to as the wave buoy analogy [23]. Tannuri et al. [24] assume prior knowledge of the RAOs to estimate vessel response using Eq.(1). The Directional Wave Spectrum (DWS) is estimated from on-board measurements of a Floating Production, Storage, and Offloading (FPSO) vessel in Dynamic Positioning (DP). The sea state parameters are then found by minimizing the quadratic error between estimated and measured vessel response.

Sea state estimation using machine learning yields benefits in terms of their independence of mathematical models such as the vessel RAOs. Algorithms are trained to recognize patterns in the measurements and thus require different information about the vessel. An example is proposed by Alfsen [25]. Using Convolutional Neural Network (CNN) based on regression and classification models, the significant wave height, peak period, an wave direction is estimated based on data from Inertial Measurement Unit (IMU) sensors.

Two approaches for estimating the relative wave direction using machine learning are proposed by Mak and Düz [26, 27]. The first approach adopts a CNN and Recurrent Neural Network (RRN) for multivariate regression from 6 DoF ship motion time series and wave measurements. Despite some shortcomings in the data, good estimates are obtained compared to established methods [26]. However, the performance depends on the training strategy of the neural networks. The second approach by Mak and Düz [27] considers various types of neural networks trained on a comprehensive simulated data set of eleven different ship geometries. The training set consists of a selection of the ships, and the neural networks are evaluated on the remaining ships. Remarkable performance is achieved by the neural networks based on the simulated data. The networks are able to generalize over geometry, yielding future potential for estimating the sea state based on a general model. However, when the trained neural networks were reused on in-service measurement data of a frigate vessel, the results depend on the selected approach. For the transfer learning approach, where the neural network is further trained on the measured data, more accurate results are obtained for the relative wave direction compared to the

direct application approach. Here, no further training of the models was obtained before being applied to the in-service measurements.

3.2 Estimation of Vessel Models

The prediction accuracy of vessel responses is limited by the corresponding wave information and vessel model accuracy. In recent decades, several studies have been made on improving response prediction by proposed sea state estimation approaches based on both first-principle models and data-driven methods. For some operational- and vessel-dependent uncertainties, reductions are normally obtained by careful design and organization of operation activities or monitoring systems. However, uncertainties related to vessel parameters such as inertia distribution and damping are challenging to measure [5]. The influence of uncertainties in vessel RAOs on the short-term response variance was assessed by a model developed by Soares [28]. The results showed that the variance uncertainty varies with vessel heading, significant wave height, and zero-up crossing period of the sea state. This indicates an existing potential in vessel model estimation to improve knowledge of on-site conditions.

One attempt to improve vessel model description in terms of the RAO is addressed by Skandali et al. [3]. An approach is proposed to calibrate the vessel RAOs by vector fitting and modification of fitting parameters based on measured vessel response and a directional wave spectrum. With the goal of decreasing the deviations between measured and predicted vessel motion, the results show an increased accuracy when discrepancies in motion prediction are caused by imprecise estimates of the vessel characteristics. However, when the discrepancies are caused by nonlinear effects such as potential mass and damping, the methodology fails due to non-convexity.

In her master thesis, Vettestad [29] proposes a parameteric and non-parametric method for RAO estimation to predict heave motions during offshore oil drilling from floating rigs or drilling ships. The methods are implemented with both measured- and modeled wave spectrum, as well as measured heave amplitude. The parametric model is modeled as a Single Input Single Output (SISO) mass-spring-damper system, while the non-parametric model is based on the relation between the heave motion, RAO amplitude, and wave spectrum, with no assumptions regarding system structure. It is shown that the methods perform differently based on the conditions. The parametric model performs best under ideal conditions, while the non-parametric model yields better results using measurements.

Another approach is proposed by Han et al. [4] to improve the RAO accuracy by tuning the important hydrodynamic model parameters based on spectral analysis, probabilistic modeling, and the discrete Bayesian updating formula. An adaptive model updates both the parameter values and their confidence quantitatively. Analyses based on a numerical model of an Offshore Supply Vessel (OSV) demonstrate the potential of the tuning approach by being fast and stable to deal with noise by considering up to four uncertain parameters. The approach performs reasonably, yielding better results for the tuned pa-

rameters, which strongly influences the measured vessel response. Similarly, updating the parameters for cases where the sea states or measurements were less critical for the uncertain parameters showed reasonable behavior. In a second paper, Han et al. [5] address a challenge with the former approach being time-consuming and computationally expensive due to the curse of dimensionality. Therefore, a novel and much more efficient algorithm for model parameters tuning is proposed to solve this problem while also being able to reduce the considered uncertainties from waves through the proposed tuning procedure. The approach is based on the unscented transformation and scaled unscented Kalman filter. This makes the approach efficient for dealing with large dimensional problems and can account for system nonlinearities. Based on a simulated case study of an OSV, the tuning results are shown to approach the true values.

Kaasen et al. [30] considers a different approach related to improved vessel model descriptions. Instead of tuning the RAOs, parameters in the SIMO[1] software are subject to automatic model tuning. The linear and square damping, stiffness, and mass are the parameters selected for tuning, based on the tuning principle of minimizing the difference between the measured and simulated response. The challenge by this approach was seen in roll response tuning for other directions than beam sea. The output error was significant with the reason being unknown. The responses in sway, heave, pitch, and yaw were improved by the tuning approach.

3.3 Prediction of Wave-induced Vessel Response

The requirement of a high level of safety for the majority of marine operations has motivated researchers to study methods for accurate calculation of the future wave-induced vessel response. In execution of operations in the nearest future, like lifting operations and helicopter landings, it is valuable to know the response minutes forward in time through short-time predictions based on previous response measurements [31]. Longer time horizons are of interest for operations like installations and pipe-laying to evaluate the vessel operability according to operational limits determined based on regulations and standards defined by class societies and national directorates [32].

Nielsen et al. [33, 31] present two methods for short-time, deterministic vessel response prediction in the nearest future from prior measurements. Both are independent of any knowledge of the environmental conditions and any offline training. Instead, they rely on the autocorrelation function. The first presented method evaluates 7200 sets of predictions and artificially simulated measurements of the vertical acceleration of a Liquefied Natural Gas (LNG) carrier, with a prediction horizon in the order 30 s. The study of mean values of the normalized Root Mean Square (RMS) value is based on predictions up to 50 s ahead of time and shows that prediction accuracy depends on the time horizon. For larger horizons from 20 s to 50 s, the accuracy reduces. Also, accuracy is highly dependent on the autocorrelation of the actual process. Particularly the degree of smoothing of the response

[1] https://www.dnv.com/services/complex-multibody-calculations-simo-2311

spectra influences the outcome.

The second study presented by Nielsen et al. [31] extends the first procedure to using experimental data obtained from model-scale tests. By considering a period of $T_{past} = 25T_p$, where T_p is the peak period, predictions are made 7.5 s ahead of the current time, corresponding to 41 s in full-scale. The study shows that the procedure effectively can be extended to full-scale measurements, yielding successful results for the given time horizon.

A prediction procedure for use in ship-helicopter flight operations based on simulated motion data is proposed by Yan et al. [34]. The algorithm models the current state observation as a linear function, where the respective orders of its previous states and system input is obtained using the Bayes Information Criterion. A comparison study of the proposed algorithm, an order-predefined predictor, and an AutoRegressive model predictor was made for a wave height of 1 m. The study shows that the method sacrifies prediction error for capacity, but overall yields satisfactory performance for use in flight operations.

Attempts to predict ship motions based on data-driven methodologies are addressed in literature. Kawan et al. [35] proposes a system structure based on Support Vector Regression (SVR) utilizing raw data for verification. The SVR model is trained and tested on 1750 and 25 data samples, respectively, and evaluated on a case study for trajectory and pitch velocity prediction. The case studies show good performance of the proposed model, yielding small values in the Root Mean Square Error (RMSE) and Square Correlation Coefficient (R^2) close to 1. Duan et al. [36] proposes another data-driven approach, where real-time estimation of deterministic ship motions are obtained based on a Long-Short-Term-Memory (LSTM) deep learning model. Based on simulated data of nonlinear ship motions and datasets of the corresponding waves, the proposed method yield comparable results with a traditional Hydrodynamic Transfer Function (HTF) method. In higher sea states, the LSTM neural network outperforms the HTF method in heave motion due to its nonlinear advantages.

Pivano et al. [37] study the digital twin performance of a semi-submersible drilling rig for use in planning DP drilling operations. The study is motivated by the many advantages of cloud-based digital twins, like increased simulation efficiency and sharing of real-time information and predictions between stakeholders. The key contribution of the study is to validate the digitial twin for drift-off simulations based on full-scale measurements from sea trials in mild weather conditions. The comparison shows sufficient agreement between the measured and simulated drift-off time.

4 Methods

The implemented methods are explained in the following sections. This entails definitions and assumptions, the datasets, the sensitivity analysis on response prediction, and the two algorithms for estimating the RAOs.

4.1 Definitions and Assumptions

The sensitivity analysis and the algorithms for estimating the RAOs are based on the following assumptions

i) The vessel response is stationary. The vessels are operating in DP having a constant heading during the measurements.

ii) β is the mean relative direction between wave direction and vessel heading.

iii) The sea state is long-crested with a constant wave spectrum in the considered period.

iv) The transfer function is stationary, with constant loading condition over the period examined.

Figure 3 shows the direction definitions. Figure 3 (a) defines the incoming wave direction θ and vessel heading ψ in North-East-Down (NED) frame. The relative wave direction β in the body-frame, represented by an x-y coordinate system, is defined in Figure 3 (b). $\beta = 0°$ and $\beta = 180°$ is following- and head sea, respectively. The wave direction is denoted as μ in the following sections.

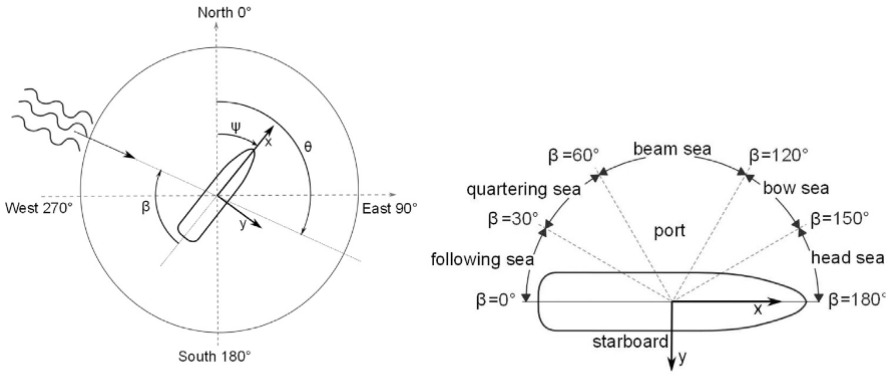

(a) Global wave propagation direction Θ (b) Relative wave direction β

Figure 3: Definition of relevant directions; θ being incoming wave direction, ψ being vessel heading, and β being the relative wave direction [38].

4.2 Datasets and Preparation

Datasets from a full-scale vessel and a model-scale vessel are used to evaluate the methods studied in this thesis. The full-scale dataset is used to study the sensitivity of response prediction to wave modeling. The study is carried out by modeling the sea state in terms of

a JONSWAP-, PM-, and an Ochi-Hubble spectrum. The experimental data obtained from model tests includes a broader range of sea states, hence will be applied to the methods for calculating a set of average RAOs that depend on a range of significant wave heights. The datasets are described in the following sections.

4.2.1 Full-scale Vessel Response Measurements

Response measurements for heave and pitch motion of a full-scale construction vessel collected during operation are provided by Subsea 7 for usage in this thesis.

Table 1 shows the main dimensions and parameters of the vessel. The dataset consists of continuous measurements of the full-scale vessel response for six months. The vessel heading, ψ, is measured by a gyrocompass in the NED reference frame. Additionally, hourly updated sea state parameters are provided by external weather forecasts. The set of parameters consists of the significant wave height, H_s, the peak period, T_p, and the wave direction, μ, for the total wave, and the wind-wave and swell component. The wind-wave and swell component is abbreviated with w and s, respectively.

Table 1: Main dimensions and parameters of the full-scale construction vessel.

Parameter	**Value**
Length, L_{pp}	151.1 m
Moulded width, B	32.0 m
Mean draught, T	8.2 m
Displacement, Δ	32 904 tons

Information about the vessel state is given in terms of keywords described in the operation log, distinguishing between working conditions and when the vessel is under transit or mobilization. Due to the weather forecast duration, a selection of 1-hour samples is chosen for which the vessel is working, assuming that the working condition implies operation in DP. Table 2 shows the chosen samples, describing the sample name, vessel heading, and corresponding predicted sea state parameters. H_s, T_p, and μ are the significant wave height, peak period, and wave direction for the total wave. Furthermore, $(H_{s,w}, H_{s,s})$, $(T_{p,w}, T_{p,s})$, and (μ_w, μ_s) represents the corresponding sea state parameters for the wind wave and swell component, respectively. The wave directions are defined such that the waves are traveling from North towards South for $\mu = 0°$, hence must be converted 180° to apply for the direction definitions in Section 4.1.

Table 2: Sample, vessel heading, and sea state parameters for the construction vessel and sea states.

Sample	ψ	H_s $(H_{s,w}, H_{s,s})$	T_p $(T_{p,w}, T_{p,s})$	$\mu(\mu_w, \mu_s)$
A	311°	1.3 (0.2, 1.2) m	11.2 (2.7, 11.2) s	205° (192°, 206°)
B	184°	1.8 (0.2, 1.8) m	13.3 (2.5, 13.5) s	198° (208°, 198°)
C	77°	1.4 (0.3, 1.4) m	14.2 (3.3, 14.4) s	214° (177°, 215°)
D	17°	1.1 (0.4, 1.1) m	15.8 (3.7, 15.9) s	206° (191°, 208°)
E	239°	0.9 (0.4, 0.8) m	11.2 (3.2, 12.3) s	210° (240°, 205°)
F	340°	1.7 (0.7, 1.6) m	12.5 (5.0, 12.3) s	350° (42°, 340°)

The samples in Table 2 are applied to the sensitivity study, and are chosen as the encountered sea states in the dataset with the most variation in spectral parameters. However, the dataset does not contain much variation during the six months of measurements, and the sea states are mild. Furthermore, it is observered that the sea states are dominated by swells with limited variations in the significant wave height, and a double-peaked wave spectrum may seem redundant since the wind-wave contribution to the spectrum will be small. Nevertheless, the individual wave parameters are included in the study to evaluate the unknown aspects of calculating the wave parameters.

4.2.2 Experimental Data from Model Test

Physical data of the vessel model Cybership Inocean Cat I Drillship (CSAD) is gathered in the test basin at the MC Lab located at the Center of Marine Technology in Trondheim. The laboratory consists of a wave basin with dimensions 40 x 6.45 m (LxB) and a water depth of 1.5 m [39, 40].

Qualisys motion capture system, towing carriage, wave generator, and a video camera are fixed equipment allowing experimental testing of marine control systems and hydrodynamic tests [39]. The Qualisys motion capture system tracks six DoF using three Oqus cameras and infrared reflector balls placed on the vessel. A real-time CompactRIO (cRIO) controller from National Instruments (NI) located in the vessel running Qualisys Track Manager [2] software reads the transmitted camera data [39, 40]. A wave-making machine generates waves with a 6-meter wide paddle. The wave generator can generate both regular and irregular waves with the capacity given in Table 3.

Table 3: Capacity of wave maker [39].

	Height [m]	**Period T [s]**
Regular waves	$H < 0.25$	$0.3 - 3.0$
Irregular waves	$H_s < 0.15$	$0.6 - 1.5$

[2] https://www.qualisys.com

CSAD is a 1:90 scaled model developed by Bjørnø in 2016 as part of his master thesis [41] and designed as an Arctic Drillship by Inocean for Statoil (now Equinor). The propulsion system consists of three azimuth thrusters in the stern and bow and is equipped with a moonpool for turret and mooring lines. The control system is programmed in Simulink and compiled to C code to run real-time by the cRIO through the software NI VeriStand [3]. The model is equipped with a SixAxis gamepad controller and Raspberry Pi 2, allowing human operator input to the control system [41]. Table 4 shows the main dimensions of CSAD and Figure 4 shows the vessel model. Since the motion RAOs of CSAD are originally unknown, the RAOs in heave and pitch are calculated in the hydrodynamic workbench, ShipX [42], based on strip-theory.

Table 4: Scaled dimensions (1:90) of C/S Inocean CAT I Drillship [41].

Description	**Full-scale data**	**Model-scale data**
Length over all, L_{oa}	232.0 m	2.578 m
Width, B	39.6 m	0.440 m
Depth moulded, D_m	19.0 m	0.211 m
Draught design, D_T	12.0 m	0.133 m

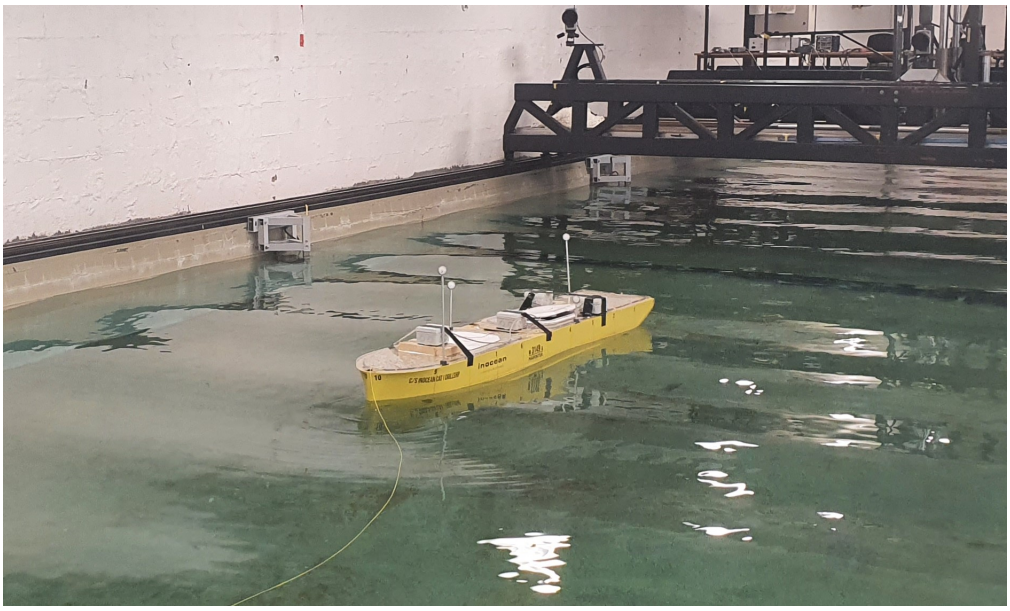

Figure 4: Test basin and CSAD in the MC Lab.

A set of test cases are chosen based on the table of realistic sea states by Price and Bishop [43]. Table 5 shows the chosen cases denoted by SS_n, with corresponding significant wave height and peak period in full-scale and model-scale. Irregular waves are modeled as a JONSWAP spectrum, and 15 minutes vessel response measurements in DP are collected

[3] https://www.ni.com

for each test case in head sea to obtain a reliable estimate of the response spectrum. The first 100 seconds are removed from the measurements to avoid any transient behavior.

Table 5: Test cases for CSAD in head sea. The significant wave height and peak period are given in full-scale and model-scale.

	Full-scale		**Model-scale (1:90)**	
SS_n	H_s	T_p	H_s	T_p
1a	1 m	7.72 s	0.011 m	0.81 s
1b	1 m	8.63 s	0.011 m	0.91 s
1c	1.5 m	7.72 s	0.017 m	0.81 s
1d	1.5 m	8.63 s	0.017 m	0.91 s
1e	1.5 m	15.84 s	0.018 m	1.67 s
1f	1.9 m	7.72 s	0.021 m	0.81 s
1g	1.9 m	8.63 s	0.021 m	0.91 s
2a	2 m	8.73 s	0.022 m	0.92 s
2b	2 m	9.57 s	0.022 m	1.01 s
2c	2.5 m	8.73 s	0.128 m	0.92 s
2d	2.5 m	9.57 s	0.128 m	1.01 s
2e	2.5 m	15.84 s	0.028 m	1.67 s
2f	2.9 m	8.73 s	0.028 m	0.92 s
2g	2.9 m	9.57 s	0.028 m	1.01 s
3a	3 m	9.65 s	0.033 m	1.02 s
3b	3 m	10.39 s	0.033 m	1.09 s
3c	3.5 m	9.65 s	0.039 m	1.02 s
3d	3.5 m	10.39 s	0.039 m	1.09 s
3e	3.5 m	15.84 s	0.039 m	1.67 s
3f	3.9 m	9.65 s	0.043 m	1.02 s
3g	3.9 m	10.39 s	0.043 m	1.09 s
4a	4 m	10.47 s	0.044 m	1.10 s
4b	4 m	11.17 s	0.044 m	1.18 s
4c	4.5 m	10.47 s	0.050 m	1.10 s
4d	4.5 m	11.17 s	0.050 m	1.18 s
4e	4.5 m	15.84 s	0.050 m	1.67 s
4f	5 m	10.47 s	0.056 m	1.10 s
4g	5 m	11.17 s	0.056 m	1.18 s

4.2.3 Froude Scaling

Representation of the data obtained from the experimental testing of CSAD in full-scale is obtained by Froude scaling. The scaling method relates the inertia and pressure forces to gravity forces by the ratio

$$F_n = \frac{V_{vessel}}{\sqrt{gL}}, \tag{29}$$

and is based upon keeping the ratio equal for the model and full-scale vessel [14]. V_{vessel} is the forward vessel speed, g is the gravitational constant, and L is the vessel length. The geometric similarity is obtained by the ratio, $\lambda = L_s/L_m$, for the full-scale vessel and the model, respectively. From a dimensionality analysis, λ, and the requirement from Eq.(29), scaling of other physical quantities is obtained by

$$\text{Length:} \quad L_s = \lambda L_m, \tag{30a}$$

$$\text{Mass:} \quad M_s = \frac{\rho_s}{\rho_m}\lambda^3 M_m, \tag{30b}$$

$$\text{Time:} \quad t_s = \sqrt{\lambda} t_m. \tag{30c}$$

The ratio ρ_s/ρ_m is used to correct for water density differences between the operational environment and test basin. Full-scale values of CSAD main dimensions in Table 4, and the sea state parameters for the test cases in Table 5, are Froude scaled based on the physical quantities in Eq.(30). Similarly, the timeseries of the response measurements from the MC Lab are Froude scaled by Eq.(30a) for heave motion, and the time is scaled by Eq.(30c).

4.3 Post-processing of Data and Preliminary Analysis

Since the algorithms for estimating the RAOs are formulated in the frequency domain, the measured time series must be transformed. The Power Spectral Density (PSD) of the vessel responses are calculated from a Discrete Fourier Transform (DFT) using the *dat2spec* function in the WAFO toolbox [44] in MATLAB[4] 2019b. The result yields information about the magnitude and phase.

Based on the sea state parameters, the wave spectra are modeled as a JONSWAP-, PM-, and an Ochi-Hubble spectrum according to the theory in Section 2.2. The input parameters for the two former spectra for the total wave are

- H_s: Significant wave height,
- T_p: Peak period,
- γ=3.3: Peak shape factor [16].

The input parameters for the Ochi-Hubble spectrum are

- $H_{s,w}$: Significant wave height for the wind component,

[4]https://se.mathworks.com

- $T_{p,w}$: Peak period for the wind component,
- $H_{s,s}$: Significant wave height for the swell component,
- $T_{p,s}$: Peak period for the swell component,
- $\lambda = 3$: Spectral shape parameter [15].

4.3.1 Data Selection of the Full-scale Measurements

Since the operation log of the construction vessel described in Section 4.2.1 do not provide detailed information about the vessel state for the period where the response measurements are collected, the measurements may be affected by unknown aspects of the ongoing operations. Therefore, the samples may not represent perfect DP conditions. This again will impact the accuracy of the results from the sensitivity study.

Figure 5 shows an example of two different 1-hour time series of the roll response while the vessel is working. The upper plot represents the roll angles for sample A described in Table 2, and the lower plot represents the measured roll angles for an arbitrary sample selected for a different day. As seen in the lower plot, the roll angle changes significantly in the first 5 minutes of the measurements before it settles at a mean value of approximately 0.3°. After about 18 minutes, the roll angle again changes to a static mean angle of 0° for the remaining part of the time series. The roll response seen in the upper plot shows steady and more significant oscillations around 0° for the whole period. The different roll behaviors in the time series can be explained by the measurements being collected for different types of operations. An ongoing lifting operation may cause the small roll response and static angles for the arbitrary sample. The metacentric height value changes during the considered time window and will deviate from the wave-induced response for a vessel with zero roll angle. Considering this as a reasonable assumption, the samples in Table 2 were chosen using the measured roll response to indicate the most representable time series of the actual vessel response encountered by the on-site sea state.

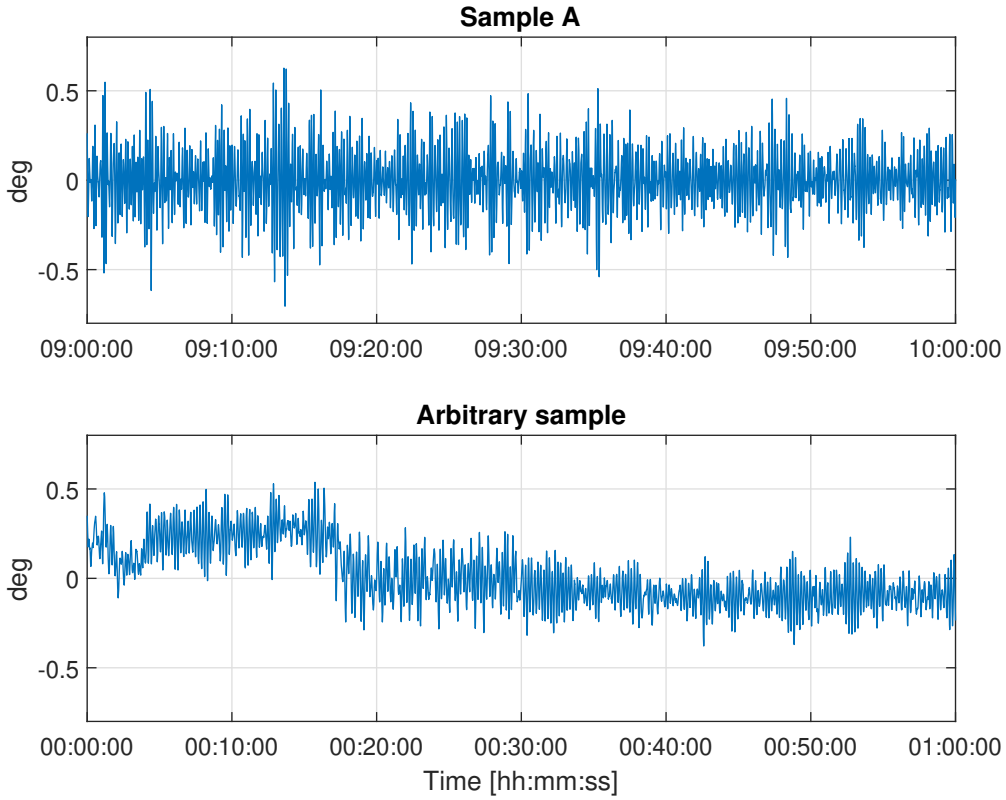

Figure 5: Timeseries of the roll response for sample A and an arbitrary sample from the dataset, measured at two different days.

Reliable response predictions require the wave spectrum to be adequately modeled by the available spectral parameters. The parameters in Table 2 yield the possibility of utilizing the total wave parameters, or the wind-wave and swell component, to model a uni-modal or bimodal wave spectrum, respectively. Although the wind-wave contribution to the total sea state is minor, the total wave parameters are not fully represented by the swell component. Furthermore, the relation between the parameters and assumptions introduced in the prediction methods by the forecasts are not known. It is therefore necessary to evaluate the total- and decomposed wave parameters to identify any potential uncertainty elements that may affect the results from the sensitivity study. This is especially important for calculating the theoretical response using the Ochi-Hubble spectrum. For long-crested waves, the correct RAOs are then chosen for the relative direction between the vessel heading and the direction of the total wave calculated from the wind-wave and swell parameters.

The wave parameters in Table 2 are evaluated and compared by calculating the total significant wave height and wave direction from the wind-wave and swell parameters. The total peak period is considered the peak period related to the dominating wave component in the sea state. A method for calculating the total wave parameters is presented by Nielsen and Dietz [45] based on the weightings

$$w_1 = \frac{H_{s,w}^2}{\overline{H_s}^2}, \tag{31a}$$

$$w_2 = \frac{H_{s,s}^2}{\overline{H_s}^2}, \tag{31b}$$

of the significant wave heights. $\overline{H_s} = \sqrt{H_{s,w}^2 + H_{s,s}^2}$ is the total significant wave height. Accounting for the circularity in wave directions, a new set of parameters

$$A = w_1 \cdot \cos(\mu_w) + w_2 \cdot \cos(\mu_s), \tag{32a}$$

$$B = w_1 \cdot \sin(\mu_w) + w_2 \cdot \sin(\mu_s), \tag{32b}$$

based on the Cartesian vector components of the particular directions is introduced [46]. The total wave direction for the wind-wave and swell component is then given as

$$\overline{\mu} = \arctan(B_k, A_k). \tag{33}$$

Table 6 shows a comparison of the total wave parameters for the wind-wave and swell components, and the total wave parameters provided in the forecast. Note that the wave directions, μ and $\overline{\mu}$, are converted according to Figure 3. The differences between the total wave parameters are minor for most of the samples. The maximum difference for the significant wave height and wave direction is 0.1 m and 2°, respectively. The most significant difference appears for the peak periods in sample E with a difference of 1.1 s. The peak period is defined as the period for which the wave spectrum has its maximum, hence the total peak period, T_p, should be equal to $\overline{T_p}$ [9]. For frequencies where the slope of the RAOs is large, such differences can yield significant changes in the wave-induced response dependent on the chosen wave modeling methods. Furthermore, the values presented in Table 6 highlight the issue of the limited information about how the spectral parameters are calculated and may introduce challenges in validating the reliability of the wave spectrum models for the considered sea states.

Table 6: Wave parameters for the total wave provided by the forecasts (H_s, T_p, μ) and calculated based on the wind-wave and swell component ($\overline{H_s}$, $\overline{T_p}$, $\overline{\mu}$)

Sample	$\boldsymbol{H_s}$	$\boldsymbol{\overline{H_s}}$	$\boldsymbol{T_p}$	$\boldsymbol{\overline{T_p}}$	$\boldsymbol{\mu}$	$\boldsymbol{\overline{\mu}}$
A	1.3 m	1.2 m	11.2 s	11.2 s	25 deg	26 deg
B	1.8 m	1.8 m	13.3 s	13.5 s	18 deg	18 deg
C	1.4 m	1.4 m	14.2 s	14.4 s	34 deg	33 deg
D	1.1 m	1.2 m	15.8 s	15.9 s	26 deg	26 deg
E	0.9 m	0.9 m	11.2 s	12.3 s	30 deg	32 deg
F	1.7 m	1.7 m	12.5 s	12.3 s	170 deg	169 deg

4.3.2 Preliminary Analysis of the Experimental Measurements

The motion RAOs of CSAD are computed in ShipX based on Computer Aided Design (CAD) drawings and linear potential theory, and are referred to as ShipX RAOs [42]. The ShipX RAOs are used for validating the experimental response spectra for the test cases in Table 5.

A selection of response spectra is presented with the RAOs and corresponding wave spectra in Figures 6 and 7. The upper plots in the figures show the wave spectra for eight different sea states with two sea states represented in each plot. The ShipX RAOs are then shown under as the blue and green curve for heave and pitch motion, respectively. The two lower plots show the frequency-domain response of the measurements for the corresponding wave spectra. It is observed from the RAOs that the PSD for the majority of the sea states is distributed over frequencies where the wave-induced vessel response is expected to be small. This is expected for frequencies higher than 0.08 Hz and 0.1 Hz where the respective heave and pitch RAO have a local minimum after reaching their maximum magnitude.

The exception is for test cases *e* with peak frequencies of 0.06 Hz. Among the other test cases, the lowest peak frequency of 0.09 Hz is given for test case *4g*, and the highest peak frequency of 0.13 Hz is given for test case *1a*, as seen in Table 5. This means that the majority of the response measurements are represented for frequencies between 0.09 Hz and 0.13 Hz. Since the dataset will be used to estimate the average RAOs for the ranges of the significant wave heights, the frequency below 0.09 Hz for each average RAO will only be represented by one test case, namely test case *e*. Ideally, the dataset should represent more sea states distributed over a broader range of frequencies for the estimated RAOs to reproduce the physics of the vessel characteristics for the low-frequency part and the high-frequency part of the RAOs. In retrospect, it would have made sense to beforehand investigate which range of frequencies the vessel would respond to.

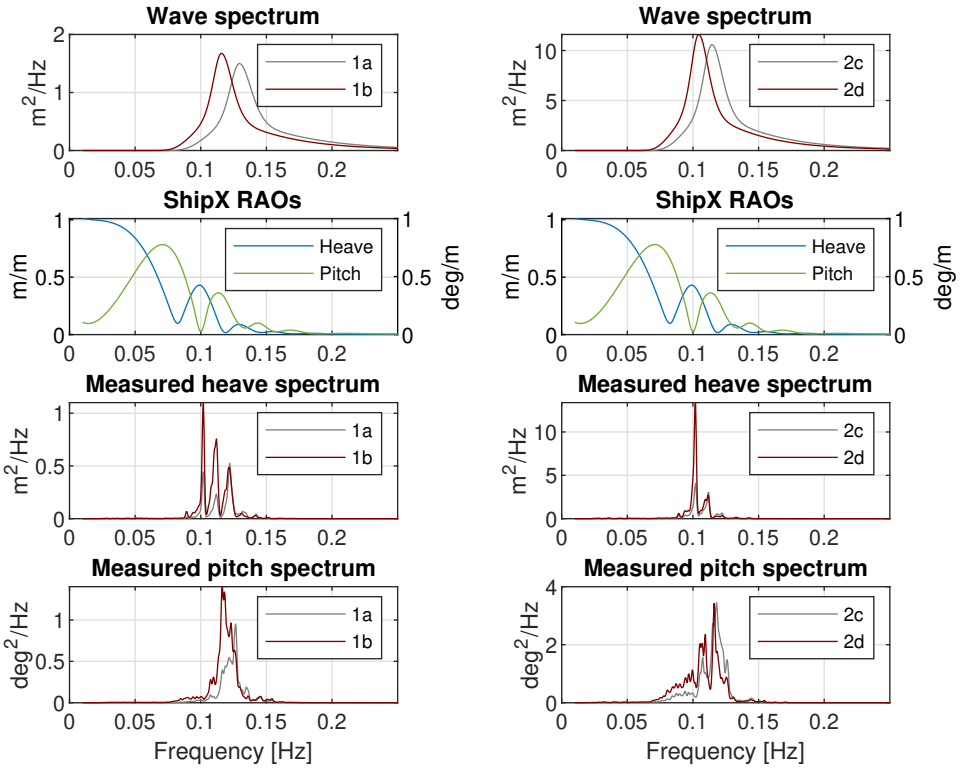

Figure 6: Wave spectrum, ShipX RAOs, and measured response spectrum for test cases 1a,b and 2c,d in Table 5.

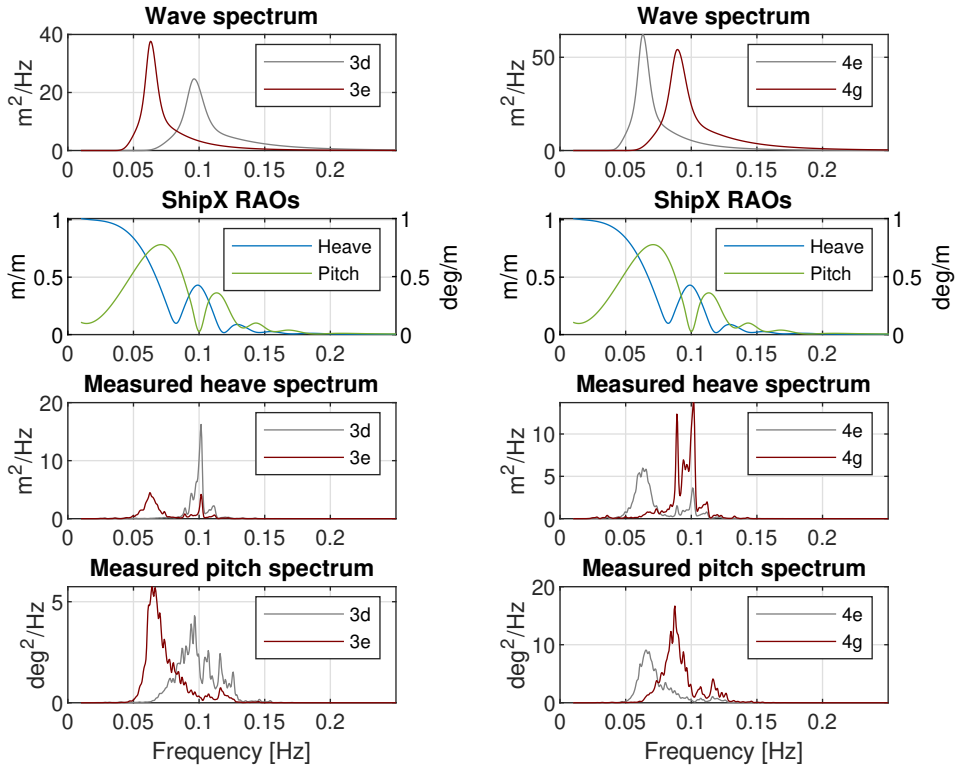

Figure 7: Wave spectrum, ShipX RAOs, and measured response spectrum for test cases 3d,e and 4e,g in Table 5.

Another observation is seen for the heave response in Figures 6 and 7. Despite the single-peaked waves represented by a JONSWAP spectrum, the response spectra for heave are multi-peaked for all test cases, except test case *3d*, where the wave peak frequency is approximately 0.1 Hz. At 0.1 Hz, a second peak in the ShipX RAO for heave yields a high and narrow peak in the response spectrum. For the other test cases where the wave energy is significantly lower at 0.1 Hz, the same spectral peak is observed. It is dominating the response for sea states with waves frequencies above 0.09 Hz, as seen for test cases *a* to *d* and *f* to *g*. In these cases, the wave energy is distributed for frequencies where the slope of the heave RAO is large, with the peak at 0.1 Hz. Therefore, the highest wave-induced response is expected to occur at this frequency.

Resonance behaviors of the water inside the moonpool of CSAD may also have contributed to the multi-peaked response observed for heave motion in Figures 6 and 7. For drilling ships like CSAD, sloshing and piston motions from the water may significantly influence the response measurements if the natural modes of oscillations are excited [47]. The former means that the water moves back and forth between the walls, while the latter yields heaving motion of the water. Simple quasi-analytical approximations to determine the natural frequencies of the moonpool via linearized potential flow theory have been derived by Molin [47]. Considering a three-dimensional problem for a barge under the assumption that the length and width of the barge are infinitely large compared to the corresponding

moonpool dimensions, the natural frequency of the piston mode is approximated as

$$\omega_{00} \approx \sqrt{\frac{g}{h + bf_3(b/l)}}, \tag{34}$$

where

$$f_3 = \frac{1}{\pi}\{\sinh^{-1}\left(\frac{l}{b}\right) + \frac{l}{b}\sinh^{-1}\left(\frac{b}{l}\right) + \frac{1}{3}\left(\frac{b}{l} + \frac{l^2}{b^2}\right) - \frac{1}{3}\left(1 + \frac{l^2}{b^2}\right)\sqrt{\frac{b^2}{l^2} + 1}\}. \tag{35}$$

In Eq.(34), the length and width of the moonpool are represented by l and b, respectively, assuming a rectangular moonpool. g is the gravitational constant. CSAD has a circular moonpool with full-scale diameter of 18 m, hence $l = b = 18$ m. This yields a natural frequency of 0.11 Hz. Given that this is an approximated value, the natural frequency yields good agreement with the peak observed at 0.1 Hz in the measured response. Therefore, it is reasonable to believe that resonance behaviors of the water inside the moonpool cause the observed peaks.

4.4 Sensitivity of Wave Modeling

A sensitivity study on vessel response prediction for the construction vessel described in Section 4.2.1 is carried out to evaluate the effect of wave spectrum modeling. The study requires prior knowledge of the RAOs and the spectral parameters of the on-site sea state, assuming perfect agreement with the true hydrodynamics of the vessel.

The wave-induced vessel response, $S_{R,i}$ for the given sea state is calculated from the linear relationship between the vessel and incoming wave as presented in Eq.(1). By considering only the motion amplitude and long-crested waves, the equation reduces to

$$S_{R,i}(\omega) = |X(\omega, \beta)|^2 S_\zeta(\omega). \tag{36}$$

Responses are calculated for $i = \{z, \theta\}$, given as heave and pitch motion, for the RAO, $|X(\omega, \beta)|$, and wave spectrum, S_ζ, at the given wave frequency, ω. Further, β is the relative wave direction.

Vessel response predictions will be obtained for the test cases in Table 2 by calculating the theoretical response for heave and pitch motion utilizing the RAO and the wave parameters modeled as a JONSWAP-, PM-, and Ochi-Hubble spectrum, according to the theory in Section 2.2. The spectra prediction capability will be evaluated by comparing the theoretical response with the response spectra computed from the measured time series. The JONSWAP- and PM spectrum will be modeled based on the spectral parameters for the total wave provided by the weather forecasts. The Ochi-Hubble spectrum utilizes the decomposed spectral parameters for the wind-wave and swell component to model the

individual contributions of the total wave. The relative wave direction for the Ochi-Hubble spectrum is obtained by calculating the total wave direction from Eq.(33), and is used to choose the correct RAOs for the theoretical response prediction. Both a JONSWAP spectrum and a PM spectrum is included in the study to evaluate the effect of not fully and fully developed seas, respectively, on vessel response prediction when the degree of development and geographical location of the sea state is unknown. Furthermore, an Ochi-Hubble spectrum will reflect uncertainties in the vessel response predictions in situations where the total wave parameters deviate from the spectral parameters for the decomposed wave components.

4.5 Tuning Algorithm

A tuning algorithm proposed by Nielsen et al. [1] has been implemented to estimate the RAOs based on available vessel response measurements, and wave spectra. It works as a simple method to obtain improved RAOs for more accurate seakeeping analyses.

The response spectrum, $S_R(\omega)$, is computed by applying a Fourier Transform on the vessel response measurements. The estimated RAO, $\hat{X}(\omega, \beta)$, is obtained by updating the initial RAO estimate, $X_0(\omega, \beta)$, based on a tuning coefficient, α_R, at wave frequencies, ω, and directions, β,

$$\hat{X}(\omega, \beta) = X_0(\omega, \beta)(1 + \alpha_R(\omega, \beta)). \tag{37}$$

For short-crested waves, the RAO estimate transfers the directional wave spectrum, $S_\zeta(\omega, \mu)$, for wave energy direction, μ, into the theoretical response estimate

$$\hat{S}_R(\omega) = \int_0^{2\pi} |\hat{X}(\omega, \beta)|^2 S_\zeta(\omega, \mu) d\mu. \tag{38}$$

Eq.(38) reduces to Eq.(36) for long-crested waves. Assuming a normal distributed residual between the measured and theoretical response estimate, $\tilde{S}_R(\omega) = S_R(\omega) - \hat{S}_R(\omega)$, the tuning coefficient is found by minimizing $\tilde{S}_R(\omega)$ for any given ω, formulated as the nonlinear unconstrained optimization problem

$$\min_{\alpha_R} \sum_{j=1}^{J} |S_R(\omega_j) - \hat{S}_R(\omega_j)|^2, \tag{39}$$

with a least-squares objective function. A reasonable initial starting value for the tuning coefficient is $\alpha_R(\omega, \beta) = 0$, i.e. $\hat{X}(\omega, \beta) = X_0(\omega, \beta)$ [1].

Seen from Eq.(38) and Eq.(39), the optimized tuning coefficient depends on the considered measured response spectrum and wave spectrum. A mean tuning coefficient calculated for a set of sequential response spectra $S_R(\omega)$ is proposed by Nielsen et al. [1]. For marine

operations restricted by specific weather requirements, it could be useful to calculate instead a set of mean tuning coefficients based on the significant wave height categorized into ranges, H, as

$$\overline{\alpha_H}(\omega, \beta) = \frac{1}{N} \sum_{n=1}^{N} \alpha_{R,n}(\omega, \beta), \tag{40}$$

where N is the number of sea states in the range.

The tuning algorithm is implemented in MATLAB 2019b, and is applied to the experimental dataset described in Section 4.2.2. For each test case, a tuning coefficient is optimized based on the Quasi-Newton BFGS method using the function *fminunc*. A mean tuning coefficient is then calculated by Eq.(40) for ranges $H = \{[1, 2]\text{m}, [2, 3]\text{m}, [3, 4]\text{m}, [4, 5]\text{m}\}$, and multiplied with $X_0(\omega, \beta)$ to obtain an updated estimate of the RAO for heave and pitch motion.

Closed-form expressions of the RAO for heave and pitch motion are calculated to serve as initial estimates of the RAOs in Eq.(37). The expressions are derived by Jensen et al. [48] based on a semi-analytical approach and require only the vessel main dimensions as input. This is restricted to length, breadth, draught, block-coefficient, waterplane area, and vessel speed and heading. The simplifications and approximations introduced in the approach yield initial estimates from which the tuning algorithm can improve and compare the results with RAOs calculated by more advanced numerical methods. A brief description of the derivation of the closed-form expressions for vertical motions is presented in Appendix A. Since zero-speed is assumed in the present study, the expressions by Jensen et al. [48] are modified to consider absolute wave frequencies, ω, rather than the encounter frequencies, ω_e.

4.6 Iterative RAO Observer

Building upon work from the pre-project submitted at NTNU in December 2020 [8], an iterative observer for estimating the RAOs has been implemented. As an extension of previous work, a set of average RAOs are calculated to depend on a pre-defined range of significant wave heights.

The observer is limited to estimate the motion RAO amplitude for long-crested waves. As similar to the sensitivity analysis in Section 4.4, the cross-spectrum in Eq.(1) then reduces to

$$S_{R,i}(\omega) = |X(\omega, \beta)|^2 S_\zeta(\omega) = A(\omega, \beta) S_\zeta(\omega), \tag{41}$$

by only considering the real parts of the transfer function. Estimates are calculated for $i = \{z, \theta\}$ given as heave and pitch motion, respectively. Further, ω is the wave frequency, and β is the relative wave direction between vessel heading and wave direction. The RAO

amplitude squared is estimated and defined as $A(\omega, \beta)$ to simplify notation. The estimation algorithm is based on an iterative approach using the residual between measured and estimated response spectra, $\tilde{S}_{R,i}(\omega, \beta)$, to calculate the estimate, $\hat{A}_i(\omega, \beta)$, given by Eq.(42a). The corresponding response spectrum is calculated by Eq.(42b).

$$\hat{A}_i{}^+(\omega, \beta) = \hat{A}_i(\omega, \beta) + k\tilde{S}_{R,i}(\omega) \tag{42a}$$

$$\hat{S}_{R,i}(\omega) = \hat{A}_i(\omega, \beta) S_\zeta(\omega) \tag{42b}$$

The updated estimate at next iteration step is given by $\hat{A}(\omega, \beta)^+$ and k is an observer gain. The sea state is represented by the wave spectrum $S_\zeta(\omega)$. A pseudocode describing the iterative algorithm is shown in Algorithm 1. For each DOF, $S_{R,i}(\omega)$ and $\tilde{S}_{R,i}(\omega)$ are initialized as the spectral amplitude of the vessel response measurement, $|S_{R,i}(\omega)|$. Furthermore, the estimates, $\hat{A}_i(\omega, \beta)$ and $\hat{S}_{R,i}(\omega)$, are initialized to zero for all frequencies N_ω. The algorithm updates the estimates in Eq.(42) and the residual until the error measure, $\max(|\tilde{S}_{R,i}(\omega)|)$, reaches a given threshold, ϵ.

Algorithm 1: Iterative scheme to estimate the RAO amplitude squared

for $i = z, \phi, \theta$ **do**
  $S_{R,i}(\omega) = |S_{R,i}(\omega)|$
  $\hat{A}_i(\omega, \beta) = zeros(1, N_\omega)$
  $\hat{S}_{R,i}(\omega) = zeros(1, N_\omega)$
  $\tilde{S}_{R,i}(\omega) = S_{R,i}(\omega)$
  while $\max(|\tilde{S}_{R,i}(\omega)|) > \epsilon$ **do**
    $\tilde{S}_{R,i}(\omega) = S_{R,i}(\omega) - \hat{S}_{R,i}(\omega)$
    $\hat{A}_i{}^+(\omega, \beta) = \hat{A}_i(\omega, \beta) + k\tilde{S}_{R,i}(\omega)$
    $\hat{S}_{R,i}(\omega) = \hat{A}_i(\omega, \beta) S_\zeta(\omega)$
  end
end

The observer algorithm estimates the RAOs for the experimental test cases described in Section 4.2.2. A set of average RAOs are then calculated for the ranges of significant wave height $H = \{[1, 2]\text{m}, [2, 3]\text{m}, [3, 4]\text{m}, [4, 5]\text{m}\}$ as

$$|\hat{X}_H(\omega, \beta)| = \sqrt{\hat{A}_H(\omega, \beta)} = \frac{1}{N} \sum_{n=1}^{N} |X_n(\omega, \beta)|, \tag{43}$$

where N is the number of testcases in H.

5 Results

This section presents the results from the sensitivity study and the algorithms for estimating the RAOs. First, the results from the sensitivity study are presented and evaluated for the full-scale dataset in Section 4.2.1. Proceeding this, the results from the proposed methods are presented for the experimental dataset in Section 4.2.2.

5.1 Results from the Sensitivity Analysis

The sensitivity of response predictions to the sea state has been evaluated by modeling the sea state using three idealized wave spectra. First, differences in the wave spectra have been discussed. Then, the theoretical responses have been calculated for each wave spectrum and compared with the measured response.

5.1.1 Wave Spectrum Modeling

Figure 8 shows a comparison of the JONSWAP-, PM-, and Ochi-Hubble wave spectrum for samples A to F as the black, yellow, and red curves, respectively. The significant wave height and the peak period for the total wave are shown for each plot's corresponding sample. It is clear from the spectral peaks that low-frequency swells dominate the sea states. Seen by the Ochi-Hubble spectra, a small contribution from the wind-wave component is only seen for sample F with a peak at 0.2 Hz. However, the contribution is minor. Thus, the power distribution is considered to be single-peaked for all Ochi-Hubble spectra and appears to be a trade-off between the JONSWAP- and PM spectra. The JONSWAP spectrum, which represents not fully developed seas, models the highest spectral peak with a narrow spectral width. The PM spectrum, on the other hand, has a lower peak and wider spectral width, yielding a PSD distributed over broader range of wave frequencies. This is expected according to the theory in Section 2.2 as the JONSWAP spectrum is a modification of the PM spectrum determined by the spectral shape parameter γ.

The difference in peak periods for the total wind-wave and the swell component for sample E is visualized in the lower-left plot in Figure 8. The Ochi-Hubble representation of the sea state yields a shifted spectrum to lower frequencies compared with the JONSWAP- and PM spectrum. Although the shift is slight for sample E, such observations indicate that predictions of the wave-induced response may be sensitive to the choice of wave spectrum for wave predictions with more significant differences in the spectral parameters. Therefore, the wave spectra and response predictions may be challenging to validate in practical applications where the actual vessel behavior is not available.

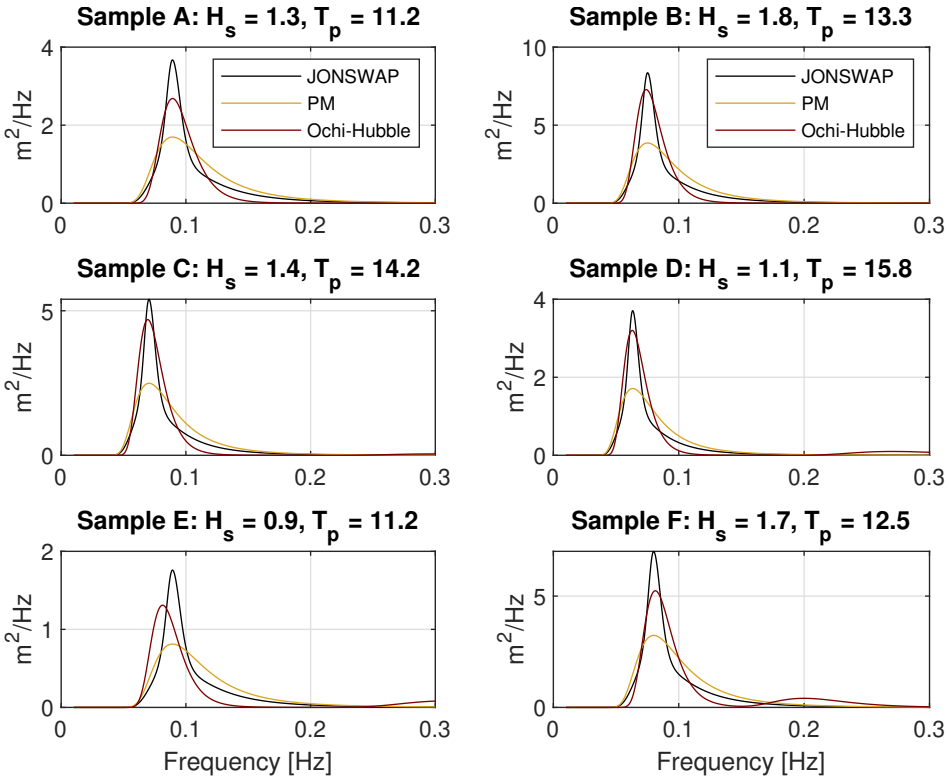

Figure 8: Comparison of wave spectra for the sea states in Table 2.

5.1.2 Theoretical Response Prediction

Table 7 shows the relative direction between the vessel heading and wave direction for samples A to F. β_μ and $\beta_{\overline{\mu}}$ is the relative direction for the total wave direction μ provided by the forecasts, and $\overline{\mu}$ calculated by Eq.(31), respectively. The directions are used to interpolate the numerically calculated RAOs to the correct relative direction for calculating the theoretical vessel responses by Eq.(36).

Table 7: Relative directions between vessel heading and waves for the samples in Table 2.

Sample	β_μ	$\beta_{\overline{\mu}}$	Description
A	73 deg	74 deg	stern-quartering sea
B	193 deg	193 deg	head sea
C	317 deg	316 deg	stern-quartering sea
D	8 deg	8 deg	following sea
E	150 deg	150 deg	beam sea
F	190 deg	189 deg	head sea

Figures 9, 10, and 11, show the wave spectrum, RAOs, and the theoretical and measured responses for samples A and B, C and D, and E and F, respectively. The responses calculated by the various wave spectra are shown by similar colors, and the gray curves

represent the measured response spectra. The theoretical responses correspond to the observed power distribution in the wave spectra, where the wave-induced response is highest for the sea states modeled as a JONSWAP spectrum. Similarly, the PM spectrum yields a lower spectral magnitude with energies distributed over a wider range of frequencies. The exception is seen in Figure 11 for heave in sample E, where the predicted response for the red curve is significantly higher than the black and yellow curves. This exception is caused by the difference in peak frequency for the wave spectra in a frequency range where the heave RAO decreases. The slope of the pitch RAO in the same frequency range is lower, so the prediction is not affected.

The response predictions based on the PM spectra yield better agreement with the measured response in both heave and pitch for samples A, B, and E. Although the theoretical responses are shifted to a lower frequency for heave in samples B and E, the power spectral magnitude and spectral width are adequate. However, for samples C and D, the measured responses are represented by a significantly more peaked and narrow spectrum. The theoretical responses underpredict the response magnitude for both heave and pitch for sample C. Furthermore, the spectral width for pitch motion is not properly represented. The same applies to the pitch motion for sample D, while the Ochi-Hubble spectrum better predicts the measured heave response magnitude. On the other hand, the second peak observed at 0.08 Hz is not captured by any theoretical responses.

The opposite observation is seen for sample F. In this case, the theoretical responses significantly overpredict the pitch motion. In contrast, the heave response is adequately predicted by both the PM spectrum and the Ochi-Hubble spectrum. It is seen by Table 7 that 3° distinguish between the relative directions for samples B and F. Thus, it is reasonable to assume that the wave-induced responses would be comparable. However, the maximum pitch response of 2 deg^2/Hz for sample F is significantly lower than 6.4 deg^2/Hz for sample B, despite the slight differences of 0.1 m and 0.005 Hz in the significant wave heights and peak frequencies, respectively. A possible explanation is that the measurements are affected by an ongoing operation at the considered period for one or both of the samples. On the other hand, an explanation for the overprediction for sample F may be that the given wave parameters do not represent the actual sea state at the considered period.

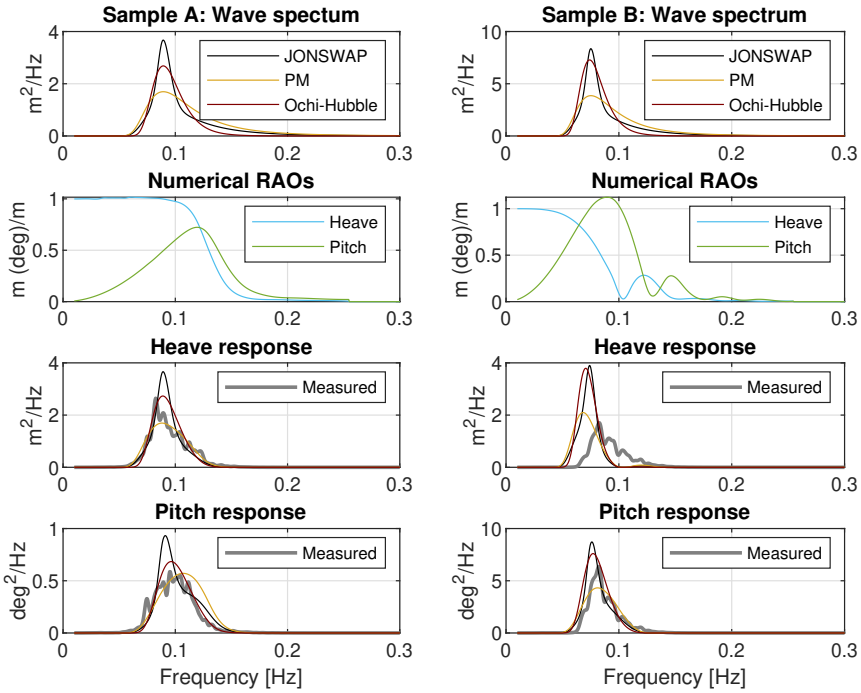

Figure 9: Measured and theoretical response for heave and pitch motion based on the JONSWAP-, PM-, and Ochi-Hubble spectrum in Figure 8.

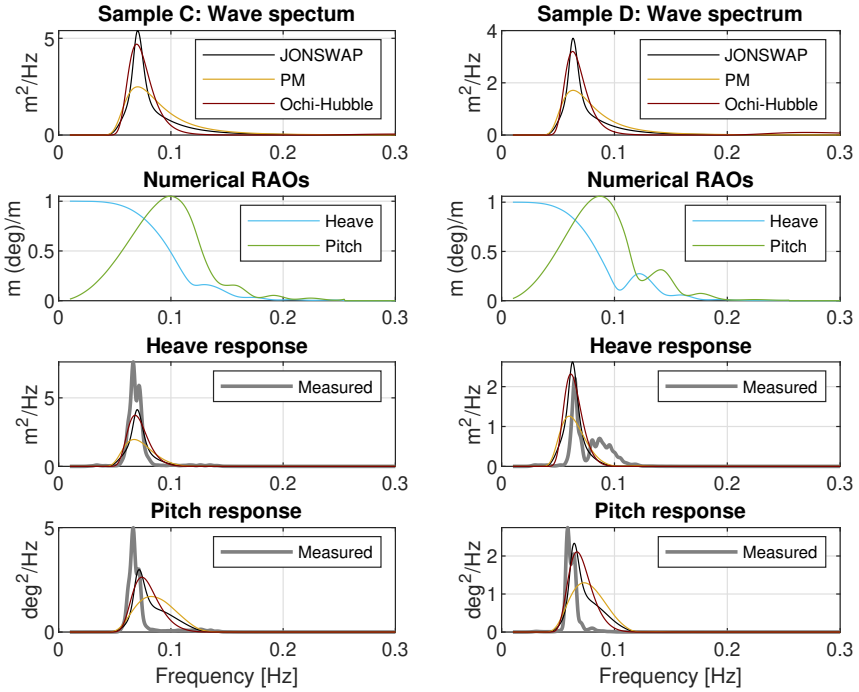

Figure 10: Measured and theoretical response for heave and pitch motion based on the JONSWAP-, PM-, and Ochi-Hubble spectrum in Figure 8.

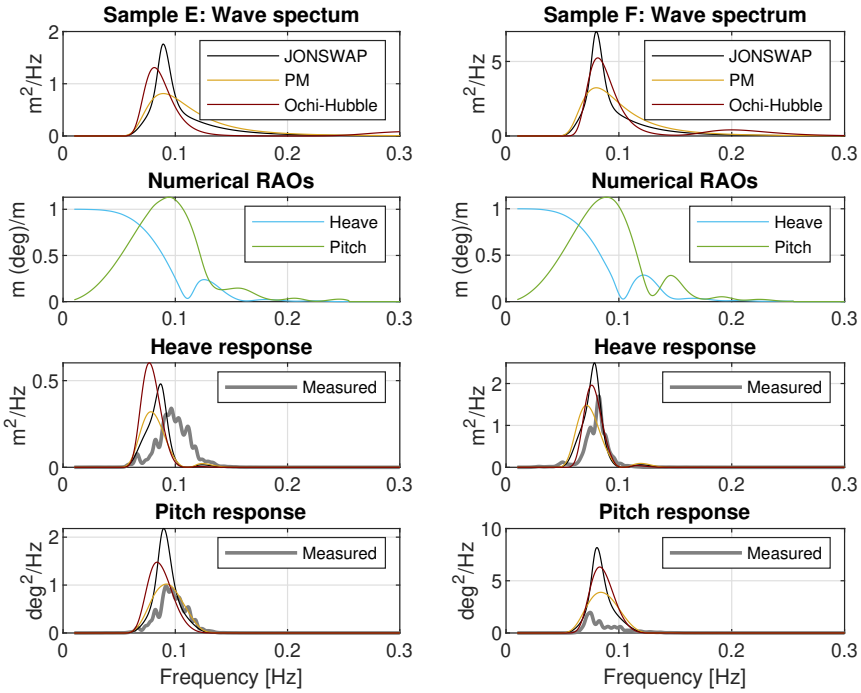

Figure 11: Measured and theoretical response for heave and pitch motion based on the JONSWAP-, PM-, and Ochi-Hubble spectrum in Figure 8.

Figure 12 shows the 0-th order spectral moment, m_0, as a function of sample, calculated for the response spectra in Figures 9, 10, and 11. As seen for heave motion in the upper plot, the Ochi-Hubble spectrum and PM spectrum generally yield the highest and lowest m_0, respectively, for the theoretical responses. The theoretical response for samples A, B, D, and E for the PM spectra show good agreement with the measured response. Sample C shows the same behavior observed in Figure 10 where the theoretical heave responses underpredict. However, it is seen by Figure 12 that the predicted response by the Ochi-Hubble spectrum achieves the best result considering the power content in the response spectra.

The theoretical responses for pitch motion show better correspondence in m_0 than for heave. The spectral moment for samples A, C, D, and E is approximately equal. However, for samples B and F, the PM spectrum shows better agreement with the measurements. The low pitch response observed in Figure 11 is highlighted in the lower plot of Figure 12 where the theoretical responses show no agreement with the measurements.

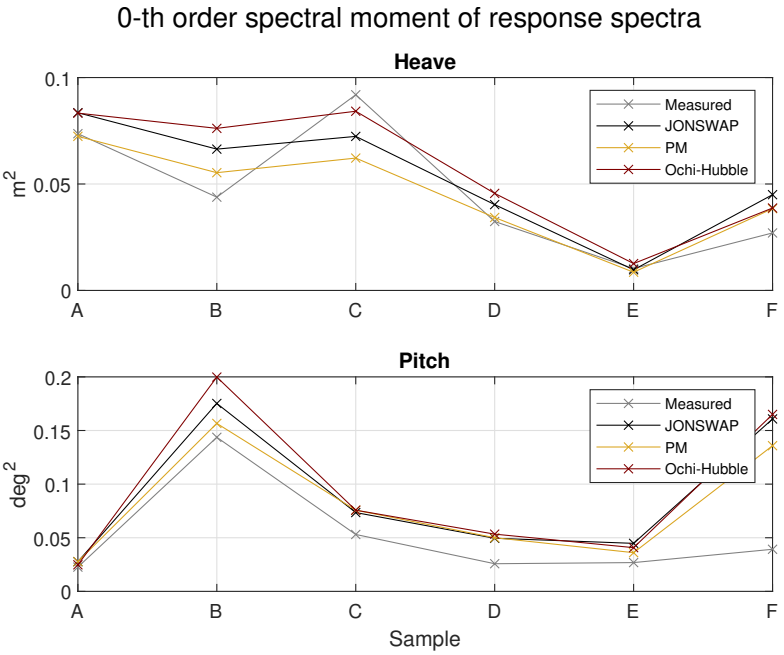

Figure 12: 0-th order spectral moment for the response spectra in Figures 9, 10, and 11.

5.2 Results from RAO Estimation

The proposed methods for estimating the RAOs have been tested and evaluated on the experimental dataset of CSAD. Based on the individual estimates obtained by the tuning- and observer algorithm from the test cases, a set of average tuning coefficients and average RAOs have been calculated by Eq.(40) and Eq.(43), respectively, based on test cases *a*, *b*, and *d* to *f*. The estimated average RAOs will be presented and discussed in this section, and their response prediction capability have been evaluated.

5.2.1 Estimation of Average RAOs

Figure 13 shows the 0-th order spectral moment calculated by Eq.(11) for the measured and theoretical response spectra at each test case. The black and yellow curve represents the theoretical estimates without and with tuning, respectively, while the red curve represents the estimate by the observer algorithm. The green curve is the spectral moment calculated using the ShipX RAOs. As Figure 13 shows, the estimates by the observer algorithm yield identical response to the measurements, given by the grey curves located behind the red curves. The use of the tuned estimates yield a small difference for all samples, but are significantly improved compared to the estimates which are not tuned. The theoretical response by the closed-form RAOs which are not tuned, and the ShipX RAOs, yield very similar results. However, the difference in the spectral moment is seen to increase for more severe sea states. The theoretical estimates underpredict the measured response for all test cases, except test cases *e*, which represents the only sea states with a peak period located in the lower part of the frequency range.

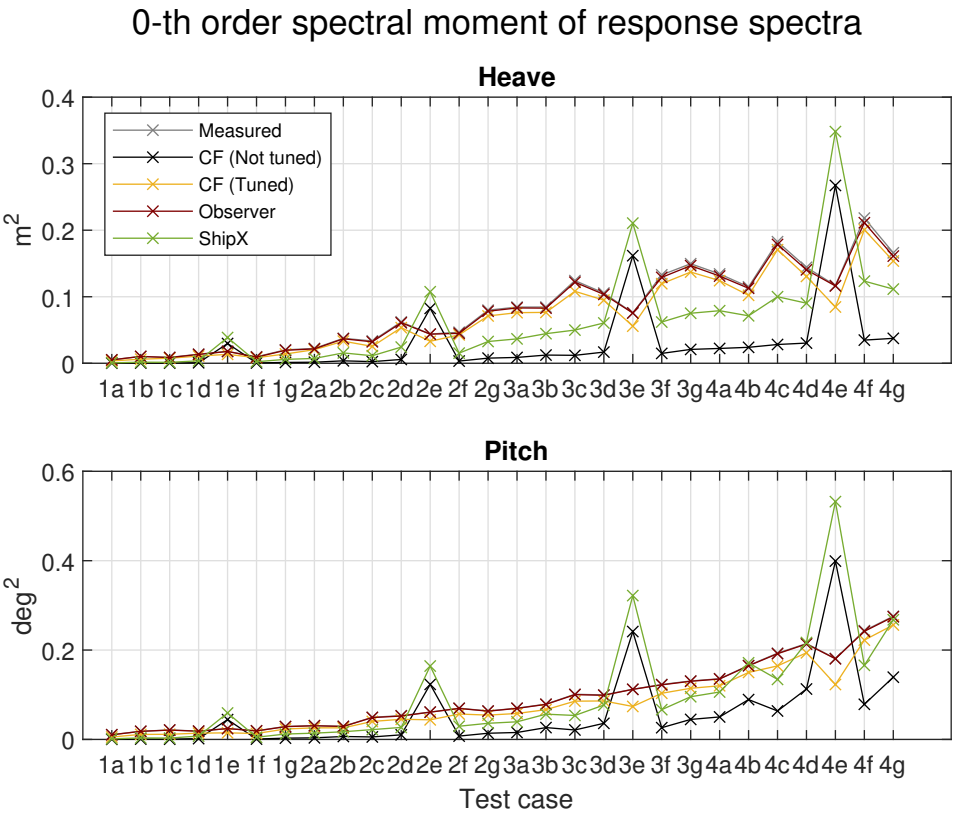

Figure 13: The 0-th order spectral moment for the measured and theoretical responses for the testcases in Table 5.

Figure 14 shows the average RAOs for heave and pitch estimated by the tuning algorithm. The results are compared with the ShipX RAO and the RAO calculated by the closed-form expressions, which is not tuned, given by the grey solid and black dotted curve, respectively. Furthermore, the average of the tuned closed-form RAOs for the range $H = \{[1, 2]\text{m}, [2, 3]\text{m}, [3, 4]\text{m}, [4, 5]\text{m}\}$ is given by the yellow, purple, green, and blue curve, respectively. Considerable tuning of the RAOs is observed for certain parts of the frequency range for both heave and pitch. The heave RAO shown in the upper plot is the most amplified for frequencies between 0.087 Hz and 0.13 Hz, which corresponds to the frequency range where most sea states are represented, as discussed in Section 4.3.2. The tuning coefficients are especially high at 0.1 Hz, yielding a peak in the estimated RAOs. This results from the same peak observed in the measured heave responses, probably caused by the moonpool resonance behavior of the water. Since the peak is present for all heave spectra independent of the sea state, and the sample-specific tuning coefficient is directly dependent on the measured response, the peak is expected to be present in the average RAOs.

The RAO for pitch motion shown by the lower plot of Figure 14 is the most amplified for frequencies between 0.1 Hz and 0.13 Hz. The resonance peak is not observed for the average pitch RAOs, but instead, a significant overprediction of the tuning coefficient with

respect to the ShipX RAO appears between 0.11 and 0.13 Hz before the tuned RAOs drop to zero. For frequencies above 0.13 Hz, the measured response spectra for both DoFs are approximately zero, hence the optimal solution of the tuning coefficient is zero, or very low, as a result of the low power content of the objective function in the optimization problem. Therefore, the tuned average RAOs coincide with the closed-form expressions which are not tuned at 0.13 Hz.

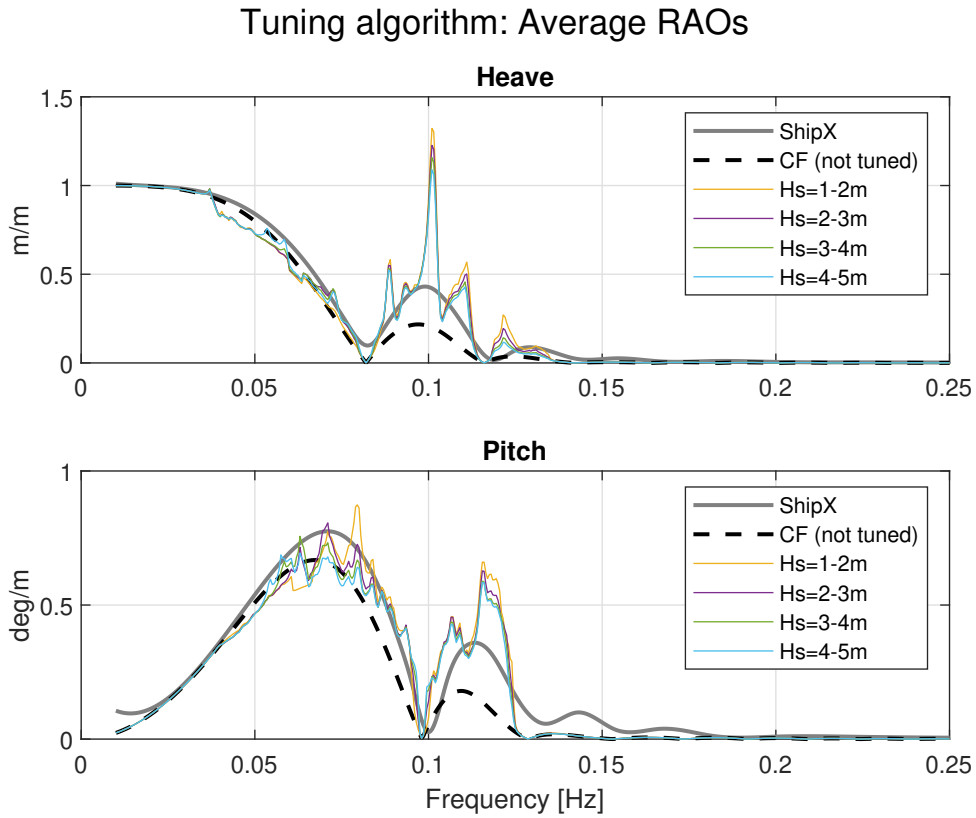

Figure 14: Estimated average RAOs by the tuning algorithm compared with the untuned closed form, and ShipX RAO in heave and pitch.

Figure 15 shows the average RAOs for heave and pitch estimated by the observer algorithm. It is clear that the estimates suffer from significant oscillations for both DoFs at low frequencies where no vessel response measurements are present in the dataset. The oscillating behavior for heave is reduced for frequencies between 0.05 Hz and 0.1 Hz. It corresponds to the frequency range where the power content of the response spectra for test cases e is distributed. For the pitch RAOs, the oscillation behavior differs depending on the range. For $H = [1, 2]$ m, no significant oscillations are observed in the estimate RAO. A reduction is observed around 0.05 Hz for $H = [4, 5]$ m, and for $H = [2, 3]$ m and $H = [3, 4]$ m a reduction occurs at 0.07 Hz. The estimated average RAOs yield better results for frequencies above 0.08 Hz and 0.1 Hz for heave and pitch, respectively. The same overpredictions seen in Figure 14 are however also present in Figure 15.

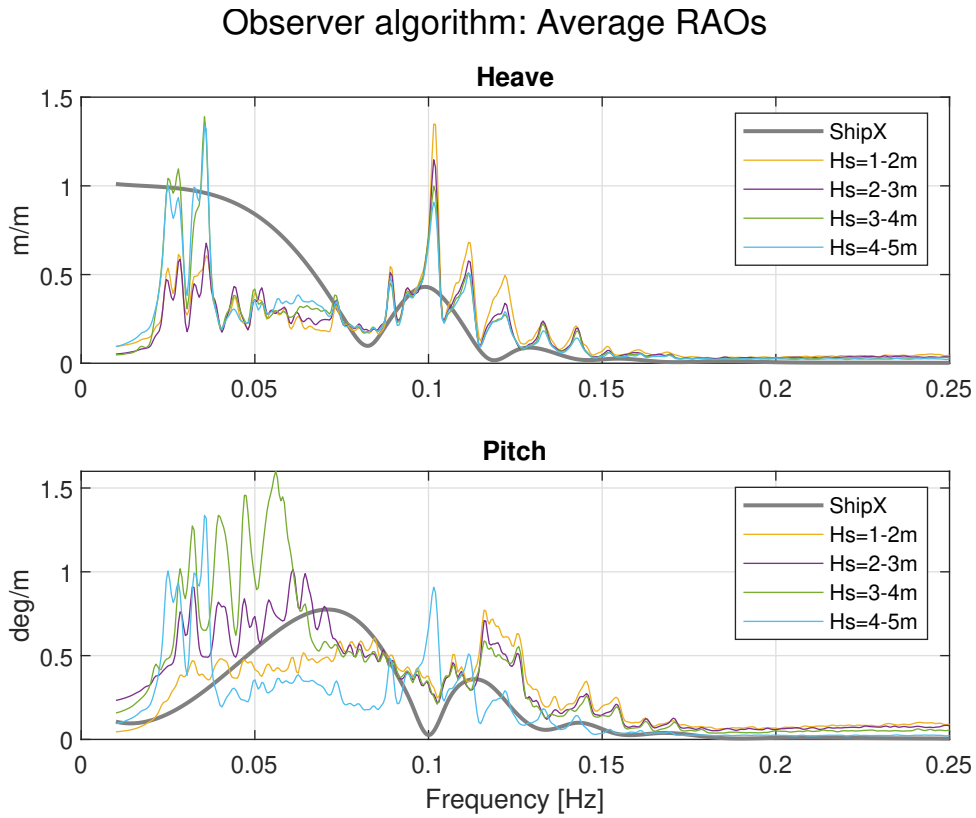

Figure 15: Average RAOs estimated by the observer algorithm compared with the ShipX RAO in heave and pitch.

As seen by Figures 14 and 15, only the pitch RAOs estimated by the observer algorithm yield significantly different results depending on the ranges of significant wave heights. Noteworthy is the average RAO for $H = [4, 5]$ m, which deviates from the other estimates for the entire frequency range. This observation is not seen in Figure 14 where the estimated pitch RAOs coincide. The difference seen in the oscillating behavior and the RAO magnitudes of the estimates indicate that the observer algorithm is more sensitive to increasing values of the significant wave height or the peak period for pitch motion. This should be investigated further through a sensitivity analysis of the methods. Furthermore, it is seen that despite very different estimates are obtained by the two methods, Figure 13 shows that the average RAOs are based on estimates with good agreement in the 0-th order spectral moment and with improved response estimates compared to the ShipX RAOs. However, it must be emphasized that the RAOs are not realistic, since the curves are expected to be smooth. This could be mitigated by including more data, or in the case of the tuning method, by imposing optimization constraints on the second derivative of the tuning coefficient with respect to frequency.

5.2.2 Response Prediction Based on Average RAOs

The prediction capability of the average RAOs estimated by the tuning- and observer algorithms have been assessed and compared by predicting the vessel response for other sea states within the corresponding range of significant wave heights. These sea states have not been included in the calculation of the average RAOs.

Figures 16 and 17 show the predicted vessel responses for test cases *c*, based on the estimated average RAOs presented in Section 5.2.1 and the known wave spectrum. The predictions have been compared with the measured response, and the theoretically calculated response with the closed-form expression of the RAOs which have not been tuned. The responses are shown by various colors in the upper and middle plots, and the lower plots show the corresponding wave spectrum. Generally, the untuned closed-form RAOs underpredict the vessel responses for both heave and pitch with nearly non-existent responses for test cases *1c* and *2c*. The responses tend to increase for increasing peak wave periods as seen for test cases *3c* and *4c*, due to the wave energy being distributed for frequencies with higher RAO magnitudes. The pitch response is adequately recreated for the two latter cases.

The predicted heave response based on the average RAOs estimated by both algorithms show good agreement with the measurements for all test cases. A difference is seen for frequencies above 0.12 Hz, where the tuning algorithm underpredicts the response. At 0.13 Hz, the predicted response obtained by the tuned RAO drops to zero before it increases again with a lower magnitude. This is caused by the observations seen in Figure 14 where the tuning algorithm estimates low RAO magnitudes for frequencies above 0.13 Hz. However, the predicted response obtained by the observer algorithm does not suffer from this underprediction due to higher magnitudes in the estimated RAO.

The same drop in predicted response at 0.13 Hz is observed for the predicted pitch response obtained by the tuning algorithm. However, in this case the predictions do not increase again at higher frequencies. Although energy content in the wave spectrum is adequate in the frequency range, the estimated RAO magnitude is approximately zero, as seen in Figure 14, and not sufficient to induce any significant vessel response. Furthermore, a similar drop is observed at 0.1 Hz. Due to the closed-form estimate of the RAO is initially zero, the estimated average RAO is also zero and cannot account for the actual vessel response in any test case.

Better response predictions for pitch are obtained by the average RAO estimated by the observer algorithm. The exception is seen for test case *4c*, which corresponds to the deviating estimate for $H = [4, 5]$ m seen in Figure 15. The peak in the RAO at 0.1 Hz yields a corresponding peak in the predicted response. However, the predicted response is significantly lower due to a local minimum in the ShipX RAO at the corresponding frequency. Additionally, the lower RAO magnitude estimated by the observer algorithm for this range is shown in the plot to underpredict the vessel response for this test case at

other frequencies.

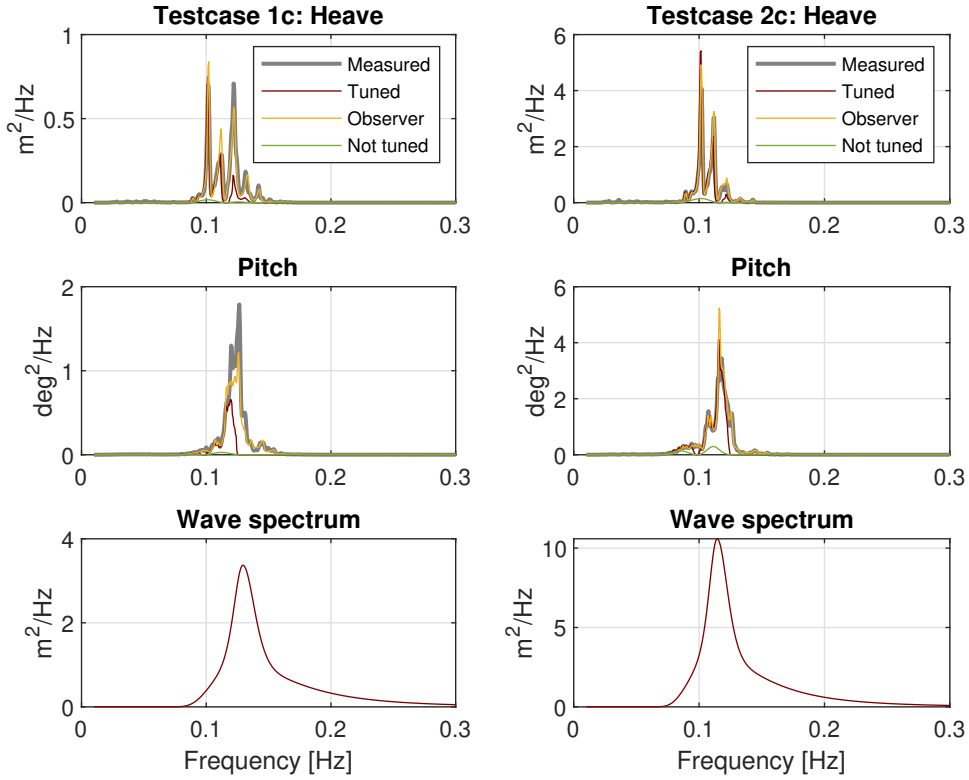

Figure 16: Predicted responses for testcases *1c* and *2c*.

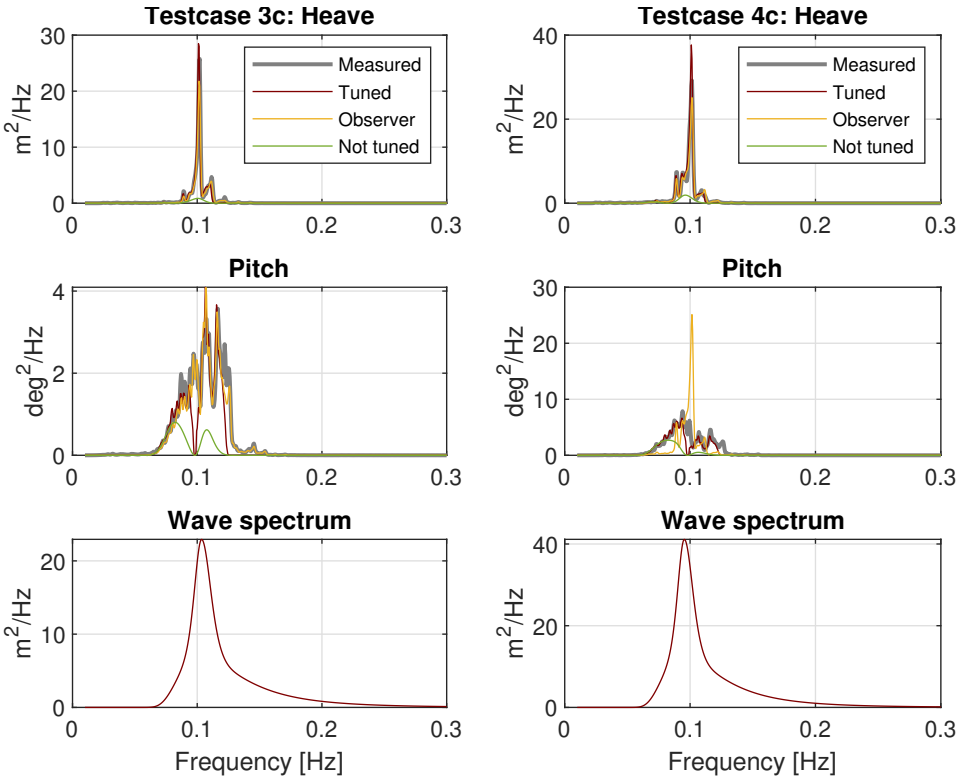

Figure 17: Predicted responses for testcases *3c* and *4c*.

Similar observations are seen in the predicted responses for test cases *g* in Figures 18 and 19. The predicted response for test case *4g* by the tuning algorithm shows good agreement with the measured response. The PSD of the measured response is fairly low at 0.1 Hz, and therefore, a drop is not seen in the predicted response for this test case. Furthermore, the PSD is distributed for frequencies below 0.13 Hz, where the estimated average RAO by the tuning algorithm yield adequate results. However, the predicted response by the observer algorithm cannot recreate the measured pitch response for test case *4g*.

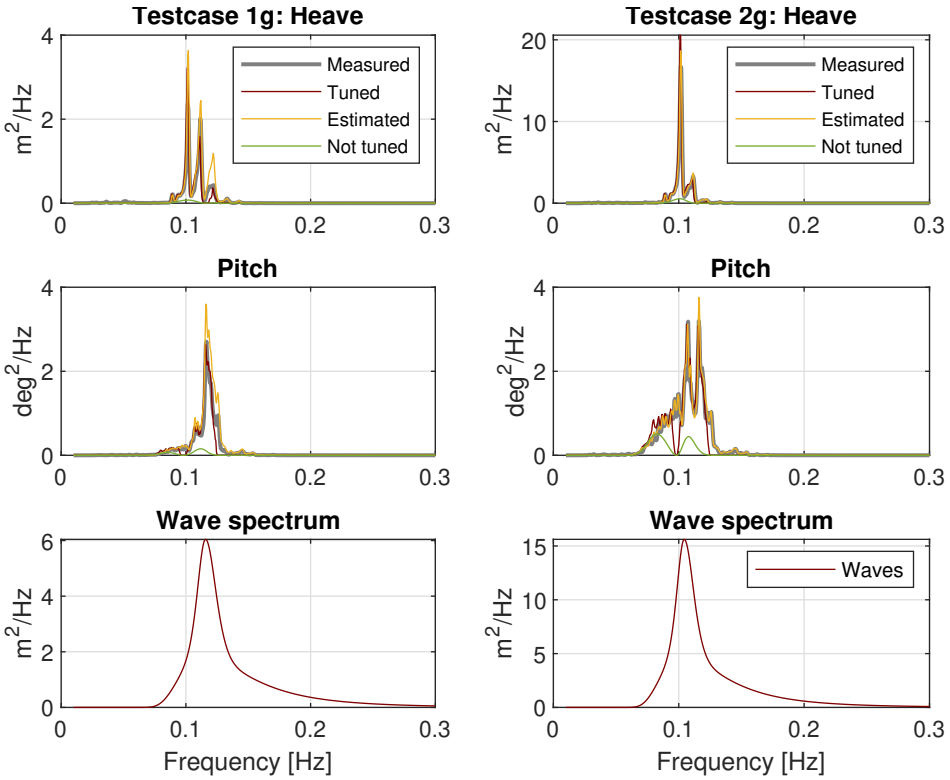

Figure 18: Predicted responses for testcases *1g* and *2g*.

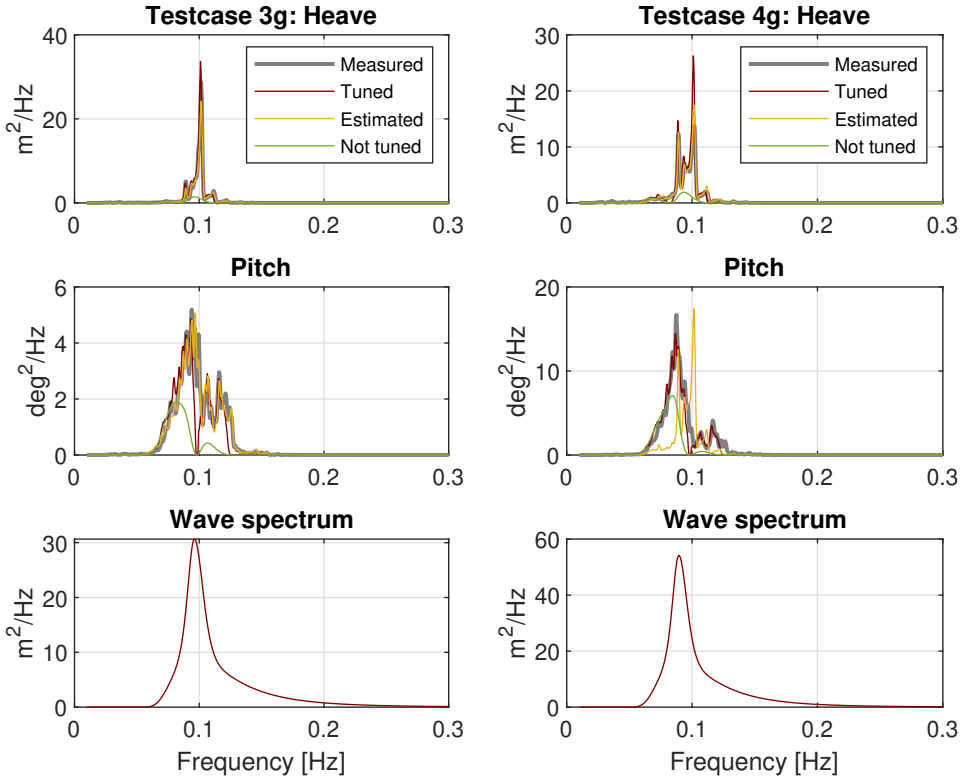

Figure 19: Predicted responses for testcases *3g* and *4g*.

6 Discussion

In examining the sensitivity study on the full-scale dataset of the construction vessel, some reflections have been made. Assuming that the vessel characteristics are fully reflected in the numerically calculated RAOs, the analyst is required to make decisions regarding the choice of wave spectrum based on a given set of wave parameters provided by an external company. This requires information and awareness of the statistical properties of the ocean environment at the specific geographical location to model the PSD of the wave spectrum correctly. It was seen in Section 5.1.2 that for some of the samples, the predicted response was influenced by the choice of wave parameters used to model the spectrum, particularly seen for sample E. Although the deviations between the 0-th order spectral moment is minor, the PSD of the wave-induced responses is sensitive to the peak period of the wave.

The uncertainties in the modeled wave spectrum for the on-site sea state are expected to be less in practical applications where information about the geographical location is available. Based on the vessel's GPS coordinates, the spectrum can be cross-validated by other forecasts or measurements at the corresponding locations, like the ERA5[5] dataset provided by the European Center of Median-Range Weather Forecasts (ECMWF). In this study where no information about the geographical location is available, the modeled wave spectra were evaluated based on the measured vessel response. However, the results from the sensitivity analysis show that although the variation in the considered sea states is small, one type of idealized spectrum is not able to yield good predictions for all samples. Despite this observation, the PM spectrum showed to provide the most adequate predictions, modeling the sea state as fully developed. This is reasonable as the contribution from the wind-wave component is small for the samples in Table 2. Thus, the JONSWAP spectrum overpredicted the spectral peak in the wave spectrum. Furthermore, the total response energy was overpredicted by the Ochi-Hubble spectrum for the majority of the sea states, seen by the 0-th order spectral moments are Figure 13. Although the parameters for the total wave, and wind-wave and swell component, are provided by the same forecast, it indicates that the parameters must be evaluated before usage to reduce the uncertainties in the response prediction.

Although the most adequate response predictions were obtained by the PM spectrum, it was seen that the prediction accuracy of the spectra differ for heave and pitch motion when comparing the theoretical and measured responses in Section 5.1.2. During operation, nonlinear effects and coupling between motions will be reflected in the measurements. Furthermore, the ongoing operations of the construction vessel is expected to have introduced significant effects in the observed response. This introduced challenges in validating the results from the sensitivity analysis based on the measured vessel responses, and it could have been beneficial to apply the study on a different type of vessel. A more accurate sensitivity analysis is expected if more samples had been considered, with

[5] https://www.ecmwf.int

a lot more variations in the sea states and less uncertainties in the operational conditions. However, the outcome of the analysis is realistic in traditional seakeeping analyses for operational scenarios of these vessels. The use of the first-principle model in Eq.(1) for response prediction in seakeeping analyses, will, based on its assumptions of linear theory, not account for such effects. Therefore, unexpected scenarios may happen since future measurements of the operation are not available for validating purposes, and uncertainties must be accounted for in advance. This means that decisions regarding waiting on weather and abortion of operations must be made on conservative predictions.

The study of the algorithms for estimating the RAOs concerns a scenario where the waves are generated based on a pre-defined wave spectrum, hence uncertainties in wave modeling can be disregarded. This makes room for the algorithms to be evaluated, and form an idea of which method that shows the most promise for future development. The estimated average RAOs in Figures 14 and 15 for the tuning and observer algorithm showed very different results, respectively. The large oscillations in the latter indicate that the observer algorithm is more sensitive to frequencies for which there is no, or almost zero, measured response. This is a result of the iterative approach based on the initial starting value of the RAOs being zero. For the same frequencies, the tuning algorithm performs significantly better based on the closed-form expressions being the initial starting value. Despite the different results and the poor similarity with the ShipX RAOs by the observer algorithm, both methods show different strengths based on their objective. The tuning algorithm may be better suited in situations where the objective is to improve existing RAOs to obtain more accurate response predictions. The observer algorithm, on the other hand, can be used to obtain estimates of the RAOs when no prior estimate is available.

The peaks in the estimated average RAOs in Figures 14 and 15 indicate that the estimates may reflect the true vessel RAOs more adequately than the ShipX RAOs by accounting for vessel behavior reflected in the considered measurements. However, the results were challenging to evaluate due to unexpected behaviors in the measured response, probably caused by resonance behaviors of the water inside the moonpool. Therefore, it would have been preferable to study the method's performances on a vessel without a moonpool.

Disregarding the uncertainties in the response measurements due to the moonpool, the peaks in the estimated RAOs also indicate that the estimates depend on the local responses. Therefore, the idea of an average RAO that is independent on the on-site conditions is not properly represented by these results, and the results do not work for their purpose. This could have been mitigated by including more data such that the average RAOs represent realistic smooth estimates, like the ShipX RAOs. Better results could also have been achieved if the dataset had represented measurements covering the entire frequency range, with the same number of test cases distributed over the frequencies, to obtain equally reliable estimated parts of the RAOs. However, this may be difficult with the considered vessel due to its large dimensions. The test basin at the MC Lab is shallow, and thus the testbed can influence the response spectra for waves with high peak periods.

Despite the questionable results obtained by the algorithms, the predicted responses for test cases c ang g, presented in Section 5.2.2, reveals that the algorithms yield improved response predictions compared to the predictions based on the RAOs which are not tuned. Especially the observer algorithm is able to recreate responses for higher frequencies where the closed-form RAOs filter out the waves. The good agreement with the measured responses was expected for test cases c and g as the sea states have their wave energy distributed for frequencies where the average RAOs are the most amplified. Therefore, it would have been interesting to evaluate the prediction capability of the average RAOs for sea states with even higher peak periods. Nevertheless, the good predictions show that the average RAOs are able to recreate the vessel responses, also for more severe sea states, and show the potential in the algorithms if more test cases had been included in the study.

Future work should be focused on including more data in both the sensitivity study and for testing and evaluating the proposed methods. The data used for the sensitivity study includes samples with small variations in the sea state, and are dominated by swells. Therefore, it may be necessary to include more severe sea states, and sea states with a higher wind sea contribution, to obtain a better representation of the wave modeling effect on the response predictions. Furthermore, the study should be extended to include spreading in the wave spectra.

In addition to including more data in the study of the tuning and observer algorithm, future work should be focused on evaluating the sensitivity of the methods with respect to the significant wave height, and include forward speed. Forward speed was applied to the tuning algorithm by Nielsen et al. [1], while only long-crested waves and zero forward speed have been considered in the observer algorithm. Further, it would be interesting to extend the scope of this thesis to combine the research objectives of the sensitivity study and the proposed methods to consider both sea state estimation and RAO estimation for cross-validating the results, and thus obtain improved vessel response predictions. Based on vessel response measurements, the uncertainties in the predictions due to the sea state and RAOs can be improved by iterative tuning. By initializing the wave spectrum based on wave parameters from a weather forecast, the RAOs can be estimated by either the tuning or observer algorithm. Following, the updated RAO estimates can be used to improve the wave spectrum through a sea state estimation approach.

7 Conclusion

The research objectives were to evaluate the response prediction sensitivity to wave spectrum modeling using three different parametrized spectra, and to generalize the RAO estimates from the proposed methods by calculating the average RAOs for a pre-defined range of significant wave heights.

7.1 Concluding Remarks

The sensitivity study has been conducted on data from a full-scale construction vessel. The study showed that the theoretical responses for heave and pitch motion are sensitive to the choice of statistical wave parameters for wave spectrum modeling. Noteworthy was the difference in peak period for the total and decomposed wave provided by the same forecast, which influenced the wave-induced response. Further, no trend was seen in the choice of idealized spectrum. Although the variation in the sea states was small, one type of idealized spectrum was not able to recreate the measured vessel response for all samples. However, the results were challenging to validate due to effects of ongoing operations reflected in the measurements.

Experimental measurements of Cybership Inocean Cat I Drillship (CSAD) have been collected from model tests, and used to evaluate the tuning and observer algorithm. The sample-specific RAO estimates showed that improved response estimates are obtained for both methods. However, the average RAOs showed a clear dependence on the local responses and did not provide realistic results, due to limitations in the dataset. The observer algorithm is volatile to low power vessel responses, observed as significant oscillations in the results. The tuning algorithm performs better since an initial estimate is assigned to the RAOs. Regardless, it has been concluded that both algorithms are promising and their use is motivated by different purposes. Despite the unrealistic behavior in the average RAO estimates, good agreement between the predicted and measured vessel response was seen for sea states with PSD similar to the sea states used in calculating the average RAOs.

7.2 Further Work

Further work should be focused on including more data for improved validation. For the sensitivity study, this considers more samples with more variation in the sea states and improved knowledge of the vessel working conditions. The study should also be conducted for another vessel for validation purposes. For the proposed methods, it considers more samples with higher peak period in the sea states. A sensitivity study of the proposed methods to the significant wave height should also be conducted.

References

[1] U.D. Nielsen, R.E.G Mounet, and A.H. Brodtkorb. "Tuning of transfer functions for analysis of wave-ship interactions". In: *Marine Structures* 79 (2021), p. 103029. ISSN: 0951-8339. DOI: https://doi.org/10.1016/j.marstruc.2021.103029.

[2] P.A. Orimolade, B.R. Furevik, and O.T. Gudmestad. "A Comparison of Wave Height Forecasts against Wave Measurements for a Location in the Barents Sea and in the Norwegian Sea". In: vol. All Days. International Ocean and Polar Engineering Conference. ISOPE-I-16-115. June 2016.

[3] D. Skandali, E. Lourens, and R.H.M. Ogink. "Calibration of response amplitude operators based on measurements of vessel motions and directional wave spectra". In: *Marine Structures* 72.102774 (2020).

[4] X. Han, B.J. Leira, and S. Sævik. "Vessel hydrodynamic model tuning by Discrete Bayesian updating using simulated onboard sensor data". In: *Ocean Engineering* 220.108407 (2021). DOI: https://doi.org/10.1016/j.oceaneng.2020.108407.

[5] X. Han et al. "Onboard tuning of vessel seakeeping model parameters and sea state characteristics". In: *Marine Structures* 78 (2021), p. 102998. ISSN: 0951-8339. DOI: https://doi.org/10.1016/j.marstruc.2021.102998.

[6] C. Gilbert, J. Browell, and D. McMillan. "A Data-driven Vessel Motion Model for Offshore Access Forecasting". In: *OCEANS 2019 - Marseille*. 2019, pp. 1–6. DOI: 10.1109/OCEANSE.2019.8867176.

[7] U.D. Nielsen et al. "Indirect Measurements of Added Wave Resistance in an In-service Container Ship". In: *proceedings of the 14th International Symposium on Practical Design of Ships and Other Floating Structures (PRADS 2019)* 63 (2021). Ed. by & K.Suzuki (eds.) T. Okada Y. Kawamura. Lecture Notes in Civil Engineering, pp. 115–132.

[8] A.H. Gjeraker. *Estimation of Response Amplitude Operators and Sea States for Vessel Response Predictions*. Pre-project written at the Department of Marine Technology at Norwegian University of Science and Technology. 2020.

[9] C.M. Larsen. *Marine Dynamics*. Ed. by W. Lian et al. Department of Marine Technology at Norwegian University of Science and Technology (NTNU), 2019.

[10] U.D. Nielsen, A.H. Brodtkorb, and A.J. Sørensen. "A brute-force spectral approach for wave estimation using measured vessel motions". In: *Marine Structures* 60 (2018), pp. 101–121. DOI: https://doi.org/10.1016/j.marstruc.2018.03.011.

[11] T.I. Fossen. *Handbook of marine craft hydrodynamics and motion control*. Ed. by T.I. Fossen. Jon Wiley & Sons, Ltd, 2011, pp. 208–210.

[12] L. Bergdahl. *Wave-Induced Loads and Ship Motions*. Department of Civil and Environmental Engineering, Division of Water Environment Technology at Chalmers University of Technology, 2009, p. 15.

[13] O.M. Faltinsen. *Sea Loads on Ships and Offshore Structures*. The Press Syndicate of the University of Cambridge, 1999, pp. 66–68.

[14] J.M.J. Journée and W.W. Massie. *Offshore Hydromechanics*. Delft University of Technology, 2001, pp. 4-6 –4-7, 6-24 –6-26.

[15] WAFO-group. *WAFO - A Matlab Toolbox for Analysis of Random Waves and Loads - A Tutorial*. Math. Stat., Center for Math. Sci., Lund Univ. Lund, Sweden, 2000.

[16] K. Hasselmann et al. *Measurements of Wind-Wave Growth and Swell Decay during the Joint North Sea Wave Project (JONSWAP)*. Deutsches Hydrographisches Institut Hamburg, 1973, p. 37.

[17] J. Nocedal and S.J. Wright. *Numerical Optimization*. Ed. by T.V. Mikosch, S.I. Resnick, and S.M. Robinson. Springer, New York, NY, 2006.

[18] C. Guedes Soares. "Effect of spectral shape uncertainty in the short term wave-induced ship responses". In: *Applied Ocean Research* 12.2 (1990), pp. 54–69. ISSN: 0141-1187. DOI: https://doi.org/10.1016/S0141-1187(05)80030-6.

[19] L. Li, S. Haver, and N. Berling. "Assessment of operational limits: Effects of uncertainties in sea state description". In: *Marine structures* 77 (2021), p. 102975. DOI: https://doi.org/10.1016/j.marstruc.2021.102975.

[20] W. Guachamin-Acero and L.Li. "Methodology for assessment of operational limits including uncertainties in wave spectral energy distribution for safe execution of marine operations". In: *Ocean Engineering* 165 (2018), pp. 184–193. DOI: https://doi.org/10.1016/j.oceaneng.2018.07.032.

[21] ITTC. *Guide in the Expression of Uncertainty in Experimental Hydrodynamicsc*. ITTC Procedure 7.5-02- 01-01 Revision 01. 2008.

[22] Y. Kim and G. Hermansky. "Uncertainties in seakeeping analysis and related loads and response procedures". In: *Ocean Engineering* 86 (2014). Uncertainty Modelling for Ships and Offshore Structures, pp. 68–81. ISSN: 0029-8018. DOI: https://doi.org/10.1016/j.oceaneng.2014.01.006.

[23] U.D. Nielsen. "A concise account of techniques available for shipboard sea state estimation". In: *Ocean Engineering* 129 (2017), pp. 352–362. ISSN: 0029-8018. DOI: https://doi.org/10.1016/j.oceaneng.2016.11.035.

[24] E.A. Tannuri et al. "Estimating directional wave spectrum based on stationary ship motion measurements". In: *Applied Ocean Research* 25.5 (2003), pp. 243–261. ISSN: 0141-1187. DOI: https://doi.org/10.1016/j.apor.2004.01.003.

[25] J.N. Alfsen. *IMU-based sea state estimation using convolutional neural networks for DP vessels*. Master Thesis. Department of Marine Technology at the Norwegian University of Science and Technology (NTNU), 2020.

[26] B. Mak and B. Düz. "Ship As a Wave Buoy: Estimating Relative Wave Direction From In-Service Ship Motion Measurements Using Machine Learning". In: vol. 9: Rodney Eatock Taylor Honoring Symposium on Marine and Offshore Hydrodynamics; Takeshi Kinoshita Honoring Symposium on Offshore Technology. International Conference on Offshore Mechanics and Arctic Engineering. V009T13A043. June 2019. DOI: 10.1115/OMAE2019-96201.

[27] B. Mak and B. Düz. "Ship As a Wave Buoy: Using Simulated Data to Train Neural Networks for Real Time Estimation of Relative Wave Direction". In: vol. 9: Rodney Eatock Taylor Honoring Symposium on Marine and Offshore Hydrodynamics; Takeshi Kinoshita Honoring Symposium on Offshore Technology. International Conference on Offshore Mechanics and Arctic Engineering. V009T13A044. June 2019. DOI: 10.1115/OMAE2019-96225.

[28] C. Guedes Soares. "Effect of transfer function uncertainty on short-term ship responses". In: *Ocean Engineering* 18.4 (1991), pp. 329–362. ISSN: 0029-8018. DOI: https://doi.org/10.1016/0029-8018(91)90018-L.

[29] M.O. Vettestad. *Response Amplitude Operator Estimation and Prediction of Heave Motions*. Master Thesis. Department of Engineering Cybernetics at the Norwegian University of Science and Technology (NTNU), 2020.

[30] K.E. Kaasen et al. "Automatic Tuning of Vessel Models Offshore: A Feasibility Study Using High-Precision Data from Model Test". In: vol. Day 2 Tue, May 05, 2020. OTC Offshore Technology Conference. D021S026R006. May 2020. DOI: 10.4043/30690-MS.

[31] U.D. Nielsen, A.H. Brodtkorb, and J.J. Jensen. "Response predictions using the observed autocorrelation function". In: *Marine Structures* 58 (2018), pp. 31–52. ISSN: 0951-8339. DOI: https://doi.org/10.1016/j.marstruc.2017.10.012.

[32] E. Sandvik, M. Gutsch, and B.E Asbjørnslett. "A simulation-based ship design methodology for evaluating susceptibility to weather-induced delays during marine operations". In: *Ship Technology Research* 65.3 (2018), pp. 137–152. DOI: https://doi.org/10.1080/09377255.2018.1473236.

[33] U.D. Nielsen and J.J. Jensen. "Deterministic Predictions of Vessel Responses Based on Past Measurements". In: vol. All Days. International Ocean and Polar Engineering Conference. ISOPE-I-17-678. June 2017.

[34] X. Yang et al. "Ship Motion Prediction for Maritime Flight Operations". In: *IFAC Proceedings Volumes* 41.2 (2008). 17th IFAC World Congress, pp. 12407–12412. ISSN: 1474-6670. DOI: https://doi.org/10.3182/20080706-5-KR-1001.02100.

[35] B. Kawan et al. "Data-driven Modeling of Ship Motion Prediction Based on Support Vector Regression". In: Proceedings of the 58th SIMS. 2017. DOI: 10.3384/ecp17138350.

[36] S. Duan et al. "A LSTM deep learning model for deterministic ship motions estimation using wave-excitation inputs". In: vol. All Days. International Ocean and Polar Engineering Conference. ISOPE-I-19-499. June 2019.

[37] L. Pivano, D.T. Nguyen, and K. Bruun Ludvigsen. "Digital Twin for Drilling Operations - Towards Cloud-Based Operational Planning". In: vol. Day 3 Wed, May 08, 2019. OTC Offshore Technology Conference. May 2019. DOI: https://doi.org/10.4043/29316-MS.

[38] A.H. Brodtkorb, U.D. Nielsen, and A.J. Sørensen. "Sea state estimation using vessel response in dynamic positioning". In: *Applied Ocean Research* 70 (2018), pp. 76–86.

[39] Department of Marine Technology at Norwegian University of Science and Technology. *Marine cybernetics laboratory handbook*. Version 2.0. 2016.

[40] Department of Marine Technology at Norwegian University of Science and Technology. *CyberShip Arctic Drillship User Manual*. 2017.

[41] J. Bjørnø. *Thruster-Assisted Position Mooring of C/S Inocean CAT I Drillship*. Master Thesis. Department of Marine Technology at Norwegian University of Science and Technology (NTNU), 2016.

[42] D.E. Fathi. *ShipX - SINTEF*. `https://www.sintef.no/en/software/shipx/`. Accessed on 06.05.2021.

[43] W.G Price. *Probabilistic theory of ship dynamics*. London: Chapman and Hall, 1974.

[44] P.A. Brodtkorb et al. "WAFO - a Matlab Toolbox for the Analysis of Random Waves and Loads". In: *Proc. 10'th Int. Offshore and Polar Eng. Conf., ISOPE, Seattle, USA*. Vol. 3. 2000, pp. 343–350.

[45] U.D. Nielsen and J. Dietz. "Estimation of sea state parameters by the wave buoy analogy with comparisons to third generation spectral wave models". In: *Ocean Engineering* 216 (2020), p. 107781. ISSN: 0029-8018. DOI: `https://doi.org/10.1016/j.oceaneng.2020.107781`.

[46] U.D. Nielsen. "Spatio-temporal variation in sea state parameters along virtual ship route paths". In: *Journal of Operational Oceanography* (2021). DOI: `https://doi.org/10.1080/1755876X.2021.1872894`.

[47] B. Molin. "On the piston and sloshing modes in moonpools". In: *Journal of Fluid Mechanics* 430 (2001), pp. 27–50. DOI: `10.1017/S0022112000002871`.

[48] J. J. Jensen, A. E. Mansour, and A. S. Olsen. "Estimation of ship motions using closed-form expressions". In: *Ocean Engineering* 31 (2004), pp. 61–85. DOI: `https://doi.org/10.1016/S0029-8018(03)00108-2`.

A Closed-form Expressions for Vertical Motions

The frequency response functions are derived using linear strip theory and neglecting the coupling terms between the motions. Assuming a homogeneously loaded box-shaped vessel, the EoM for heave, z, and pitch, θ, are written in terms of Eq.(44a) and Eq.(44b), respectively [48].

$$2\frac{kT}{\omega^2}\ddot{z} + \frac{A^2}{kB\alpha^3\omega}\dot{z} + z = aF\cos(\omega) \tag{44a}$$

$$2\frac{kT}{\omega^2}\ddot{\theta} + \frac{A^2}{kB\alpha^3\omega}\dot{\theta} + \theta = aG\sin(\omega) \tag{44b}$$

Here, B and T is the breadth and draught of the vessel, and k is the wavenumber. Furthermore, A is an approximation of the sectional hydrodynamic damping, modeled by the dimensionless ratio between the incoming and diffracted wave amplitudes

$$A = 2\sin(\frac{\omega^2 B}{2g})\exp(-\frac{\omega^2 T}{g}) = 2\sin(\frac{1}{2}kB\alpha^2)\exp(-kT\alpha^2). \tag{45}$$

The parameter α is defined in terms of the Froude number, $Fn = V/\sqrt{(gL)}$, and L as

$$\alpha = 1 - Fn\sqrt{kL}\cos\beta. \tag{46}$$

F and G in Eq.(44) is the forcing function in heave and pitch, respectively, given as

$$F = \kappa f\frac{2}{k_e L}\sin(\frac{k_e L}{2}), \tag{47a}$$

$$G = \kappa f\frac{24}{(k_e L)^2 L}\left[\sin(\frac{k_e L}{2}) - \frac{k_e L}{2}\cos(\frac{k_e L}{2})\right]. \tag{47b}$$

The effective wave number, k_e, Smith's correction factor, κ, and f are given by

$$k_e = |k\cos\beta|, \tag{48a}$$

$$\kappa = \exp(-kT), \tag{48b}$$

$$f = \sqrt{(1-kT)^2 + \left(\frac{A^2}{kB\alpha^3}\right)^2}. \tag{48c}$$

The frequency response functions for heave and pitch are given as the solution of Eq.(44a) and Eq.(44b), respectively, as

$$\Phi_w = \eta F, \tag{49a}$$

$$\Phi_\theta = \eta G, \tag{49b}$$

$$\eta = \left(\sqrt{(1 - 2kT\alpha^2)^2 + \left(\frac{A^2}{kB\alpha^2} \right)^2} \right)^{-1}. \tag{49c}$$

The shape effect of the hull geometry of a vessel is accounted for by defining the breadth by the means of C_b

$$B = B_0 C_b. \tag{50}$$

The homogeneously loaded box is modified by Eq.(50) so that the ship's total mass equals the buoyancy. Here B_0 is the maximum waterline breadth.